Please cite this article in press as: Pelissier et al., Age-Related Dysfunction in Mechanotransduction Impairs Differentiation of Human Mammary Epithelial Progenitors, Cell Reports (2014), http://dx.doi.org/10.1016/j.celrep.2014.05.021

Cell Reports
Article

Age-Related Dysfunction in Mechanotransduction Impairs Differentiation of Human Mammary Epithelial Progenitors

Fanny A. Pelissier,[1,2] James C. Garbe,[1] Badriprasad Ananthanarayanan,[4] Masaru Miyano,[1] ChunHan Lin,[1,3] Tiina Jokela,[1,2] Sanjay Kumar,[4] Martha R. Stampfer,[1] James B. Lorens,[2] and Mark A. LaBarge[1,*]
[1]Life Science Division, Lawrence Berkeley National Laboratory, Berkeley, CA 94720, USA
[2]Center for Cancer Biomarkers, Department of Biomedicine, University of Bergen, Bergen 5009, Norway
[3]Department of Comparative Biochemistry
[4]Department of Bioengineering
University of California, Berkeley, Berkeley, CA 94720, USA
*Correspondence: malabarge@lbl.gov
http://dx.doi.org/10.1016/j.celrep.2014.05.021

SUMMARY

Dysfunctional progenitor and luminal cells with acquired basal cell properties accumulate during human mammary epithelial aging for reasons not understood. Multipotent progenitors from women aged <30 years were exposed to a physiologically relevant range of matrix elastic modulus (stiffness). Increased stiffness causes a differentiation bias towards myoepithelial cells while reducing production of luminal cells and progenitor maintenance. Lineage representation in progenitors from women >55 years is unaffected by physiological stiffness changes. Efficient activation of Hippo pathway transducers YAP and TAZ is required for the modulus-dependent myoepithelial/basal bias in younger progenitors. In older progenitors, YAP and TAZ are activated only when stressed with extraphysiologically stiff matrices, which bias differentiation towards luminal-like phenotypes. In vivo YAP is primarily active in myoepithelia of younger breasts, but localization and activity increases in luminal cells with age. Thus, aging phenotypes of mammary epithelia may arise partly because alterations in Hippo pathway activation impair microenvironment-directed differentiation and lineage specificity.

INTRODUCTION

The aging process is often correlated with changes in stem cell activity with consequences ranging from reduced regenerative capacity to increased cancer incidence. Human hematopoietic stem cells accumulate with age (Kuranda et al., 2011; Pang et al., 2011) and exhibit a differentiation bias toward defective myeloid lineages (Cho et al., 2008), making individuals more prone to autoimmune problems and myeloid leukemias (Henry et al., 2011). In mice, the proportion of mitotic neural stem cells increases with age, whereas numbers of adult-born neurons decrease (Stoll et al., 2011). Human hippocampus shows patterns of age-related changes similar to mice that may underlie age-related cognitive decline (Knoth et al., 2010). Transit amplifying cells, not stem cells, accumulate in epidermis with age and delay wound healing (Charruyer et al., 2009). Mammary epithelium is maintained by a hierarchy of lineage-biased and multipotent progenitor and stem cells (Nguyen et al., 2014; Rios et al., 2014; Villadsen et al., 2007). In human mammary gland, differentiation-defective cKit-expressing multipotent progenitors (MPPs) accumulate with age, and proportions of daughter myoepithelial (MEP) and luminal epithelial (LEP) cells shift with age. We hypothesized that these age-associated changes make aged breast tissue susceptible to malignant progression (Garbe et al., 2012). Accumulation of defective stem or progenitor cells may be a common phenotype among aging tissues, and we hypothesize that aged MPPs accumulate because they do not correctly perceive microenvironmental differentiation cues.

The molecular composition of microenvironments impose specific cell fate decisions in normal and immortal nonmalignant mammary MPP (LaBarge et al., 2009). Cell culture substrata tuned to elastic moduli that mimicked normal breast tissue also biased the differentiation of an immortal nonmalignant MPP cell line into LEP (Lui et al., 2012). Matrix stiffness is mechanistically important in breast cancer progression as well; rigid breast tissue correlates with high breast cancer risk and drives malignant phenotypes in breast cancer cell lines (Yu et al., 2011). The physiological range of elastic modulus in breast likely plays an instructive role in the differentiation of normal mammary epithelial progenitors.

Membrane and cytoskeleton proteins sense mechanical cues and trigger transduction cascades that relay information throughout the cytoskeleton and to the nucleus. Responses can include changes in morphology and gene expression (Vogel and Sheetz, 2006). Sensing matrix elasticity occurs through cell-cell and cell-extracellular matrix (ECM) interactions mediated by adherens, integrins, vinculin, focal adhesion kinase (FAK), and others (Beningo et al., 2001; Bershadsky et al., 2003; Tamada

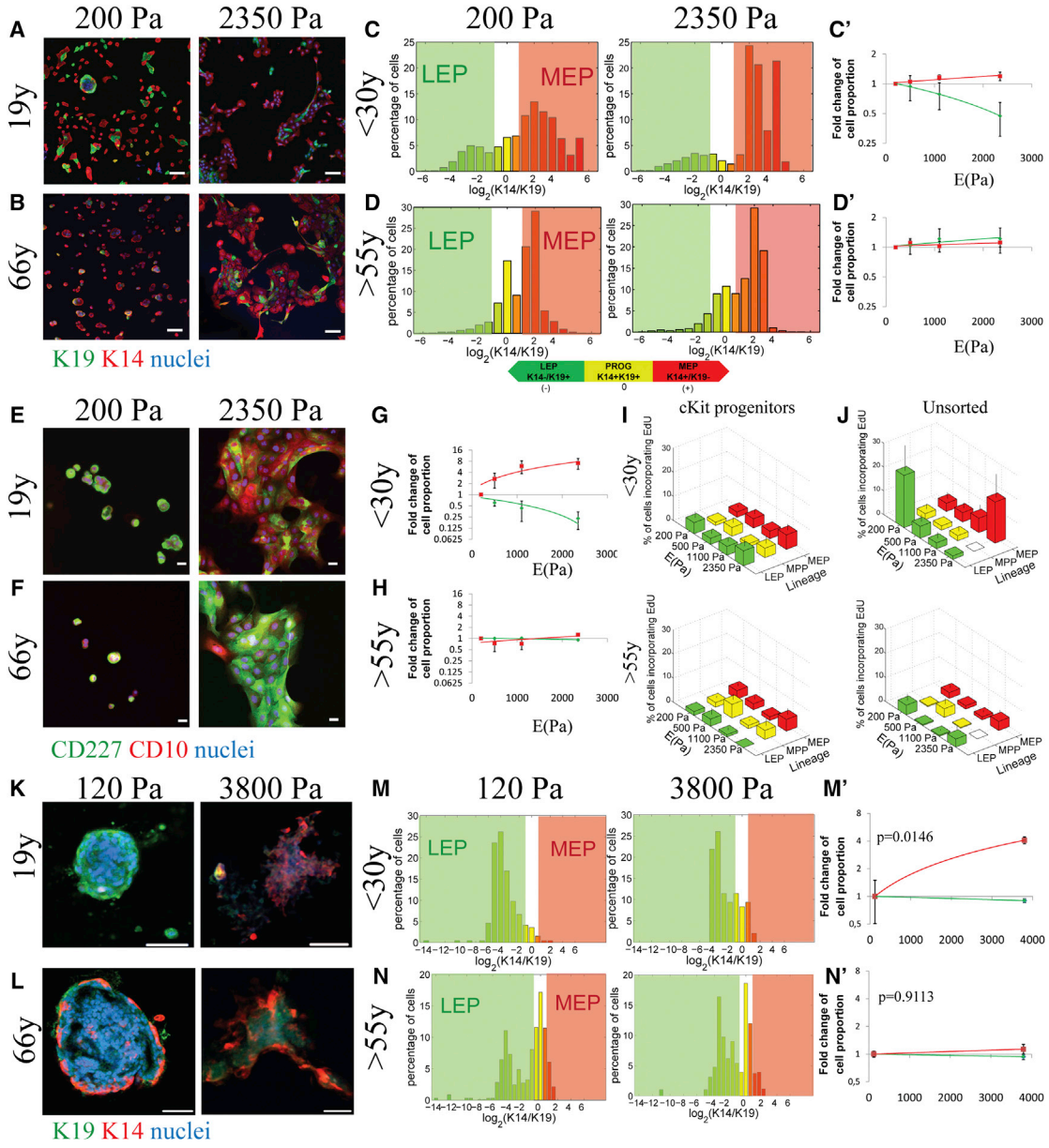

Figure 1. Aging Alters Differentiation Patterns in Response to Matrix Stiffness

(A and B) Representative IF images of progenitors from young (240L; 19 years) and (B) an older (122L; 66 years) strains stained for K19 (green), K14 (red), and DAPI (blue) after 48 hr of culture on PA gels with increasing elastic modulus (E[Pa]). Bars represent 100 μm.

(C and D) Histograms represent $\log_2$-transformed ratios of K14 to K19 protein expression in single cells on 2D PA gels with increasing stiffness; histograms are heat mapped to indicate cells with the phenotypes of K14−/K19+ LEPs (green), K14+/K19+ progenitors (yellow), and K14+/K19− MEPs (red).

(C' and D') Corresponding linear regression plots of LEP and MEP proportions as a function of modulus are shown for (C') women <30 years (LEP: $p = 0.0429$, $r^2 = 0.2086$; MEP: $p = 0.0475$, $r^2 = 0.2009$, $n = 5$) and (D') women >55 years (LEP: $p = 0.4812$, $r^2 = 0.0296$; MEP: $p = 0.5138$, $r^2 = 0.0240$, $n = 5$). Regressions are fold change of lineage proportions compared to cKit+ on 200 Pa condition ± SEM.

(E and F) Representative IF images of progenitors from (E) young (240L; 19 years) and (F) older (122L; 66 years) strains stained for CD227 (green), CD10 (red), and DAPI (blue) after 48 hr of culture on PA gels with increasing elastic modulus. Bars represent 20 μm.

(G and H) Linear regression of fold change of LEP (CD227+/CD10−) and MEP (CD227−/CD10+) proportions as function of elastic modulus in (G) women <30 years (LEP: $p = 0.0080$, $r^2 = 0.5219$; MEP: $p = 0.0198$, $r^2 = 0.4340$, $n = 3$) and (H) women >55 years (LEP: $p = 0.4689$, $r^2 = 0.0536$; MEP: $p = 0.1937$, $r^2 = 0.5219$, $n = 3$). Linear regressions are of fold change of lineage proportions normal to 200 Pa condition ± SEM.

(I and J) Percentage of cells incorporating EdU as function of lineages and stiffness in (I) cKit+ HMEC and (J) unsorted HMEC (MEP from women <30 years linear regression, $p = 0.0270$, $r^2 = 0.9467$; LEP from women <30 years t test 200 Pa versus 2,350 Pa, $p = 0.0153$, $n = 5$). Data are means ± SEM.

(K and L) Representative IF of K19 (green), K14 (red), and DAPI (blue) of passage 1 cKit+ HMEC from a 19-year-old and a 65-year-old woman after 7 days of culture encapsulated in 3D hyaluronic acid (HA) gels. Bars represent 20 μm.

(legend continued on next page)

et al., 2004). The actinomyosin network includes RhoA, which regulates the actin cytoskeleton in the formation of stress fibers (SFs) and focal adhesions (FAs). Activation of ROCK1/ROCK2 causes increased activity of the motor protein myosin II by phosphorylation of the myosin light chain (MLC) and inactivation of the MLC phosphatase (Ishizaki et al., 1997; Kimura et al., 1996). YAP and TAZ are Hippo pathway transcriptional coactivators that are thought to interact with the Rho pathway to transduce mechanical information about the microenvironment to the nucleus (Halder et al., 2012). As stiffness increases, YAP/TAZ relocates from cytoplasm into nucleus, where they generate gene expression patterns that underlie cellular functions like proliferation, migration, epithelial-to-mesenchymal transition, and differentiation (Dupont et al., 2011; Kanai et al., 2000; Zhao et al., 2007).

Differentiation of mesenchymal stem cells down neurogenic, myogenic, or osteogenic pathways was directed by exposure to a wide range of tissue-relevant elastic moduli, from 100 to ~40,000 Pa (Engler et al., 2006). In comparison, mammary MPP differentiation should be responsive to a much narrower range of modulus relevant to normal and malignant breast (100~4,000 Pa; Paszek et al., 2005). The impact of aging on modulus-directed differentiation is unknown. Addressing these issues required a culture-based platform for functional analyses of primary normal human mammary MPP from many individuals. Here, we used such an approach to demonstrate that differentiation patterns of MPP from women aged <30 years cultured on tunable 2D and 3D substrata were exquisitely responsive to a physiologically relevant range of elastic modulus in a YAP/TAZ-dependent manner, whereas MPP from women >55 years were relatively unresponsive to changes in rigidity due to inefficient activation of the Hippo pathway transducers.

RESULTS

Aging Alters Modulus-Dependent Differentiation

To test whether microenvironment rigidity directed differentiation in MPP, we enriched receptor tyrosine kinase cKit-expressing (cKit+) human mammary epithelial cells (HMECs) by flow cytometry (fluorescence-activated cell sorting [FACS]) from fourth passage primary prestasis HMEC (strains) derived from five women aged <30 years and five from women >55 years (Figure S1; Table S1). Prestasis HMEC strains are normal and not treated with any immortalizing agents, have finite lifespans, and we previously demonstrated that they retain molecular, biochemical, and functional properties consistent with chronological aging in vivo (Garbe et al., 2012). The cKit+ MPP were cultured for 48 hr on type 1 collagen-coated polyacrylamide (PA) gels. The Young's elastic modulus (E[Pa]scals) of the PA gels was tuned from 200 Pa to 2,350 Pa. The lineage of each daughter cell was confirmed by immunofluorescence (IF) of intermediate filament proteins keratin (K)14 and K19, CD227 (sialomucin-1), and CD10 (Calla; Figures 1A, 1B, 1E, and 1F). Computer image analysis identified the different lineages; LEP are $CD227^+/CD10^-/K14^-/K19^+$, MEP are $CD227^-/CD10^+/K14^+/K19^-$, and $K14^+K19^+$ expression is consistent with MPP states (Villadsen et al., 2007). cKit+ MPP from women <30 years generated proportionately more LEP on soft substrata, but generation of MEP increased with higher E (Figures 1C, 1C', 1G, and S2A). cKit+ MPP from women >55 years did not generate different lineage proportions in response to changes in E (Figures 1D, 1D', 1H, and S2B). Primary first passage cKit+ MPP from three women <30 years, embedded in tunable 3D hydrogels with some type 1 collagen for 7 days (Figure S3A; Ananthanarayanan et al., 2011), gave rise to more LEP at 120 Pa versus more MEP at 3,800 Pa (Figures 1K, 1M, 1M', and S3B). In contrast, cKit+ MPP from three women >55 years did not display modulus-dependent differentiation patterns (Figures 1L, 1N, 1N', and S3C). The proportion of $K14^+/K19^+$ MPP decreased with elastic modulus on 2D PA gels and in 3D gels <30 years HMEC (Figures S4A–S4C), but no change in proportions of MPP was observed in >55 years HMEC (Figures S4B, S4D, and S4F). These results suggested that differentiation was modulus dependent in younger MPP and that this response was lost with age.

To test if changes in lineage proportions were due to lineage-biased proliferation, incorporation of 5-ethynyl-2′-deoxyuridine (EdU) into DNA was measured as a proxy for proliferation. All lineages derived after 48 hr from cKit+ MPP on PA gels exhibited similar proportions of EdU incorporation (EdU^+), irrespective of substrate rigidity or age (Figure 1I). In contrast, EdU incorporation in unsorted HMEC strains, which are primarily composed of more mature LEP and MEP, revealed age- and lineage-specific replicative behaviors. Proportions of EdU^+ MEP from <30 years HMEC significantly increased with greater E whereas EdU^+ LEP trended downward (Figure 1J). Unsorted HMEC from women >55 years exhibited neither lineage- nor modulus-dependent proliferation (Figure 1J), underscoring the lack of mechanoresponse with age. Thus, changes in lineage proportions exhibited by <30 years MPP after 48 hr were likely due to modulus-dependent differentiation, and only after the lineages matured in <30 years HMEC strains, did they show evidence of modulus-dependent proliferation.

Mechanosensing Functions Were Unaltered by Age

To determine whether mechanosensing was age dependent, F-actin SF formation and FA assembly activities were measured in cKit+ MPP from three <30 years and three >55 years strains. Irrespective of age, SF formation increased with greater E (Figure 2A). Homogeneity measurements were used to quantify formation of the F-actin cables (Haralick et al., 1973; Pantic et al., 2012); SF homogeneity was inversely proportional to E in both age groups, which showed similar slopes (Figures 2B and 2C). Progenitors from both age groups were stained for pFAK and vinculin, which colocalize at FA. More FA assemblies were observed with increased E at the interfaces of MPP and gels, and FA

(M and N) Histograms represent $\log_2$-transformed ratios of K14 to K19 protein expression in single cells in 3D HA gels; histograms are heat mapped to indicate cells with the phenotypes of K14−/K19+ LEPs (green), K14+/K19+ progenitors (yellow), and K14+/K19− MEPs (red).
(M' and N') Fold changes of lineage proportions normal to 120 Pa condition (chi-square test women <30 years, $p = 0.0146$; women >55 years, $p = 0.9113$).
See also Figures S2, S3, and S4 and Table S2.

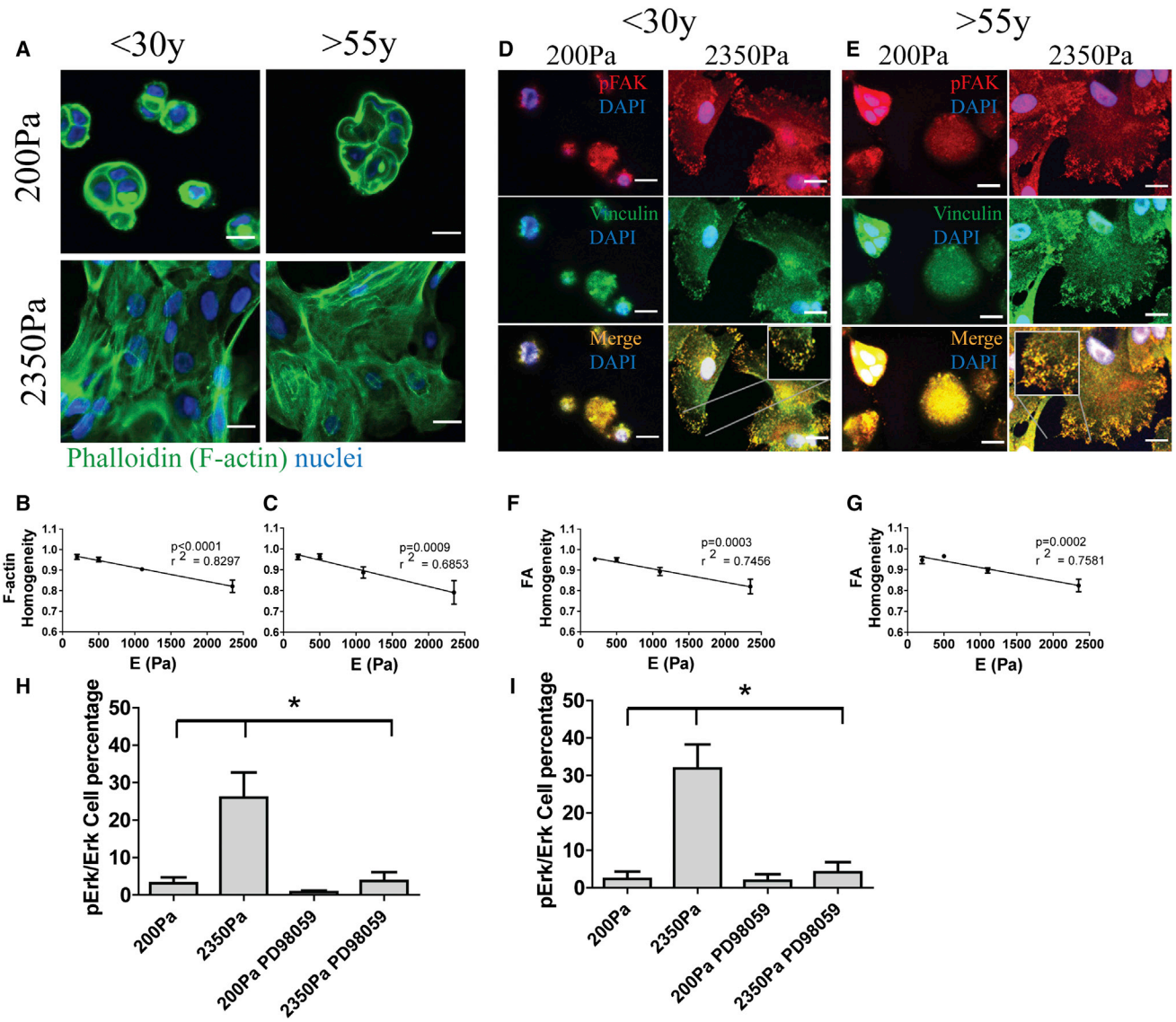

Figure 2. Mechanosensing Apparatuses Function Independently of Age to Generate Actin Stress Fibers, Focal Adhesions, and ERK Activation

(A) Representative IF images of F-actin (green) in cKit+ HMEC from a young strain (240L; 19 years) and an older strain (122L; 66 years) on PA gels of increasing stiffness.

(B and C) Quantification of F-actin homogeneity using feature detection (B, $p < 0.0001$ and $r^2 = 0.8297$, slope = $-6.805 \times 10^{-5} \pm 9.749 \times 10^{-6}$, n = 3; C, $p < 0.001$ and $r^2 = 0.6853$, slope = $-8.454 \times 10^{-5} \pm 1.811 \times 10^{-5}$, n = 3). The slopes are not significantly different (p = 0.5699).

(D and E) Representative IF images of pFAK (red) and vinculin (green), which overlapped (yellow), from confocal microscopy are shown in cKit+ HMEC from (D) a young strain (240L; 19 years) and (E) an older strain (122L; 66 years). Cells are shown at the substrata interface. Bars represent 20 μm.

(F and G) Quantification of vinculin and pFAK homogeneity (F, $p < 0.001$ and $r^2 = 0.7456$, slope = $-6.512 \times 10^{-5} \pm 1.203 \times 10^{-5}$, n = 3; G, $p < 0.001$ and $r^2 = 0.7581$, slope = $-6.356 \times 10^{-5} \pm 1.136 \times 10^{-5}$, n = 3). The slopes are not significantly different (p = 0.8124). Data are means ± SEM.

(H and I) Ratio of pERK positive to ERK positive cell number in cKit+ HMEC from <30 years (n = 3) and >55 years (n = 3) strains on 200 Pa and 2,350 Pa.

formation was not impaired with age (Figures 2D and 2E). FA homogeneity was inversely proportional to E with comparable slopes in both age groups (Figures 2F and 2G). Thus, similar SF and FA phenotypes were observed both in younger and older cKit+ MPP.

Extracellular signal-regulated kinase (ERK) is phosphorylated in response to increased elastic modulus in some adherent cell lines (Provenzano et al., 2009), and because it is a key effector of serum responses, changes in its modulation could cause pleiotropic cellular responses. Both young and old cKit+ MPP exhibited a low level of ERK phosphorylation on 200 Pa PA gels but increased up to 15-fold on 2,350 Pa PA gels (Figures 2H and 2I). Differences in pERK were not significant between age groups, and mitogen-activated protein kinase (MAPK)

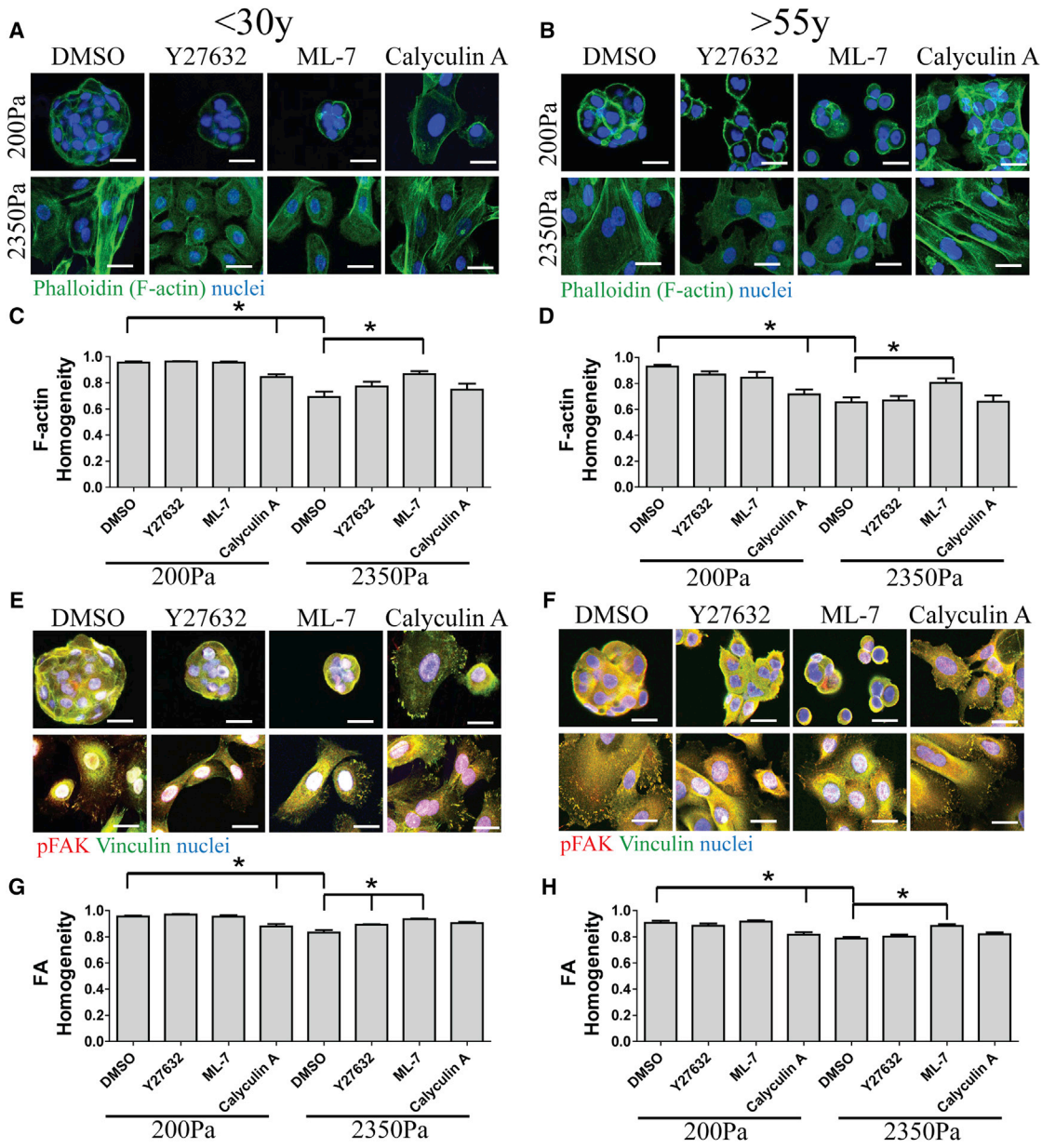

Figure 3. Perturbations of Actinomyosin Regulators Elicit Parallel Phenotypes in Progenitors from Young and Old Age Groups

(A and B) Representative IF images of F-actin with phalloidin (green) in cKit+ HMEC from (A) a young strain (240L; 19 years) and (B) an older strain (122L; 66 years).

(C and D) Quantification of F-actin homogeneity in (C) younger cKit+ (n = 3) and (D) older cKit+ (n = 3).

(E and F) Merged images of IF of pFAK (red) and vinculin (green), overlap is (yellow), in cKit+ HMEC from (E) the young strain and (F) the older strain. Bars represent 20 μm.

(G and H) Quantification of vinculin and pFAK homogeneity in (G) young cKit+ (n = 3) and (H) older cKit (n = 3).

See also Figure S5.

inhibitor PD98059 prevented ERK phosphorylation. By these measures, modulus-dependent activity in serum response was independent of age.

If mechanosensing was unaffected by aging, then perturbations of actinomyosin regulators that are known to alter FA or SF formation should elicit parallel phenotypes in young and old MPP. Independent of age, we observed that inhibitors of ROCK1/ROCK2 (Y27632) and MLC kinase (ML-7) tended to disrupt SF on 2,350 Pa substrata and showed little effect at 200 Pa, whereas the MLC phosphatase inhibitor calyculin A (calA) caused SF formation at 200 Pa (Figures 3A and 3B). Patterns of changes in F-actin homogeneity were parallel in both age groups (Figures 3C and 3D). Y27632 and ML-7 disrupted the FA assemblies on 2,350 Pa substrata, whereas calA promoted FA assembly on 200 Pa substrata (Figures 3E and 3F) and measurements of FA homogeneity showed parallel changes

Please cite this article in press as: Pelissier et al., Age-Related Dysfunction in Mechanotransduction Impairs Differentiation of Human Mammary Epithelial Progenitors, Cell Reports (2014), http://dx.doi.org/10.1016/j.celrep.2014.05.021

in both age groups (Figures 3G and 3H). Mechanosensing of substrata in the physiologically relevant range was age independent, evaluated by these measures, and thus was unlikely to account for age-dependent differences in mechanically directed differentiation.

Analysis of the effects of actinomyosin network modulation on differentiation in three young and three old cKit+ MPP revealed surprising age-dependent responses. FA and SF in cells treated with Y27632 and ML-7 on 2,350 Pa gels were similar to untreated cells on 200 Pa gels, whereas calA increased the SF and FA as if cells were on stiffer substrata. Thus, SF and FA phenotypes were pharmacologically manipulated irrespective of the actual substrate E. Younger cKit+ MPP treated with Y27632 or ML-7 significantly increased proportions of K19+ LEP compared to DMSO-treated cells on 2,350 Pa gels. In contrast, older MPP were unaffected by Y27632 or ML-7 treatment (Figure S5). Interestingly, calA increased MEP generation from young MPP but caused older MPP to give rise to significantly more LEP. No changes in proportion were observed on 200 Pa gels, suggesting that addition of calA was insufficient to trigger cell differentiation on such a soft substrata. Older progenitors did not respond to chemically decreased perception of stiffness, but they responded to artificially higher stiffness oppositely to that of young progenitors, suggesting that age-dependent transcriptional programs were operative.

Aging Alters the Ability of YAP and TAZ to Transduce Mechanical Information to the Nucleus

We next determined whether the mechanotransducive transcription factors YAP and TAZ were involved in modulus-dependent differentiation. IF staining of YAP and TAZ in cKit+ MPP from three HMEC strains <30 years exhibited increased YAP/TAZ nuclear translocation as PA gel E increased from 200 to 2,350 Pa (Figures 4A and 4B). However, significant nuclear translocation of YAP/TAZ was not observed in older progenitors in the same range (Figures 4C and 4D). The ability to activate YAP/TAZ by changes in substrate E was age dependent.

To determine the extent to which YAP/TAZ was unresponsive to changes in E in older progenitors, we evaluated their activation in response to extraphysiological stiffness. cKit+ MPP from three young and three old strains were cultured on type 1 collagen-coated glass (>3 GigaPa) or 200 Pa gels. YAP/TAZ translocated to the nucleus in young cKit+ MPP on glass (Figures 4A and 4B), gave rise to fewer LEP (Figure 4E), and those LEP incorporated less EdU on glass compared to 200 Pa gels (Figure 4F). In older cKit+ MPP on glass, YAP/TAZ was nuclear (Figures 4C and 4D), but cells gave rise to more LEP (Figure 4G), which incorporated more EdU on glass than on 200 Pa gels (Figure 4H). Both calA treatment and culture on extraphysiologically rigid substrata elicited more LEP differentiation in older MPP, which was the opposite of younger MPP. Thus, the Hippo pathway mechanoresponse in older progenitors was shifted to an extraphysiological "trigger point".

To determine if YAP and TAZ were required for modulus-dependent differentiation, both in the physiological and extraphysiological ranges, cKit+ MPP were transfected with small interfering RNAs (siRNAs), siYAP or siTAZ, which achieved >70% knockdown of the respective mRNAs (Figure 4K). K14 and K19 proteins were measured by IF in each cell after 48 hr on PA gels. Younger MPP harboring either siYAP or siTAZ were unable to give rise to more MEP on 2,350 Pa PA gels and glass substrata compared to controls (Figure 4I). In older MPP, siYAP and siTAZ had no effect at 200 Pa or 2,350 Pa, but they prevented the generation of more LEP on glass (Figure 4J). Thus, YAP and TAZ were required for modulus-dependent differentiation in progenitors irrespective of age.

YAP Localization Changes with Age In Vivo

That YAP and TAZ activity correlated with a bias toward MEP in younger women prompted us to evaluate normal breast tissue sections from reduction mammoplasty. K14, K19, and YAP were evaluated by IF in sections from four women aged 34 years, 40 years, 50 years, and 54 years (Figure 5A). Multiple fields from each section were analyzed to account for heterogeneity, and marker-based watershed cell segmentation identified levels of YAP in nuclear and cytoplasmic domains of MEP, LEP, and K14+/K19+ putative MPP. YAP staining was localized mainly to the nuclei of MEP and MPP in the 34 years and 40 years glands (Figure 5B). In the 34 years gland, we also observed a number of occurrences of K14+/K19− cells that we assumed were LEP based on their luminal location. Upon measuring the YAP signal intensity, it was determined that the K14+ cells always correlated with higher YAP expression (Figure 5C). In contrast to younger epithelia, the 50 years and 54 years glands exhibited no inequality in YAP localization between the different lineages (Figure 5B), and qualitatively, the even-appearing distribution of YAP in the nuclei and cytoplasm of the LEP and MEP in older women was reminiscent of YAP staining in >55 years HMEC (Figure 5C). YAP distribution in vivo was age dependent consistent with our findings in primary cultures. Overall, the data suggest that YAP activity is associated with MEP/basal phenotypes, even in the case of LEP in older women that acquire some traits of MEP. That impression was strengthened by our analysis of breast cancer data from The Cancer Genome Atlas data (Cancer Genome Atlas, 2012), which showed that YAP/TAZ mRNA expression negatively correlated with levels of LEP-related proteins and mRNAs and positively correlated with markers of MEP and with YAP/TAZ target genes (Figures S6A and S6B).

Levels of Hippo Pathway Components Changed with Age

To better understand why the trigger point for YAP/TAZ was increased in older MPP, we determined whether Hippo pathway components showed age-dependent expression patterns. Mst1/Mst2, Lats2, and angiomotins (AMOT) phosphorylate and sequester YAP/TAZ in the cytoplasm, which would prevent YAP/TAZ from associating with DNA-binding cofactors TEAD1–TEAD4 and transcribing target genes, like connective tissue growth factor (CTGF) (Zhao et al., 2007, 2011). Analysis with quantitative real-time PCR (qRT-PCR) revealed that, in almost all cases, *MST1/MST2*, *LATS2*, *AMOT, AMOTL1, TEAD1–TEAD4,* and *CTGF* were significantly correlated between women <30 years and women >55 years on 200 Pa (Figure 6A; $p = 0.0110$; $R = 0.7283$) and 2,350 Pa (Figure 6B; $p = 0.0083$; $R = 0.7464$) gels. On glass, the correlation was less pronounced (Figure 6C; $p = 0.0543$; $R = 0.5934$). Because

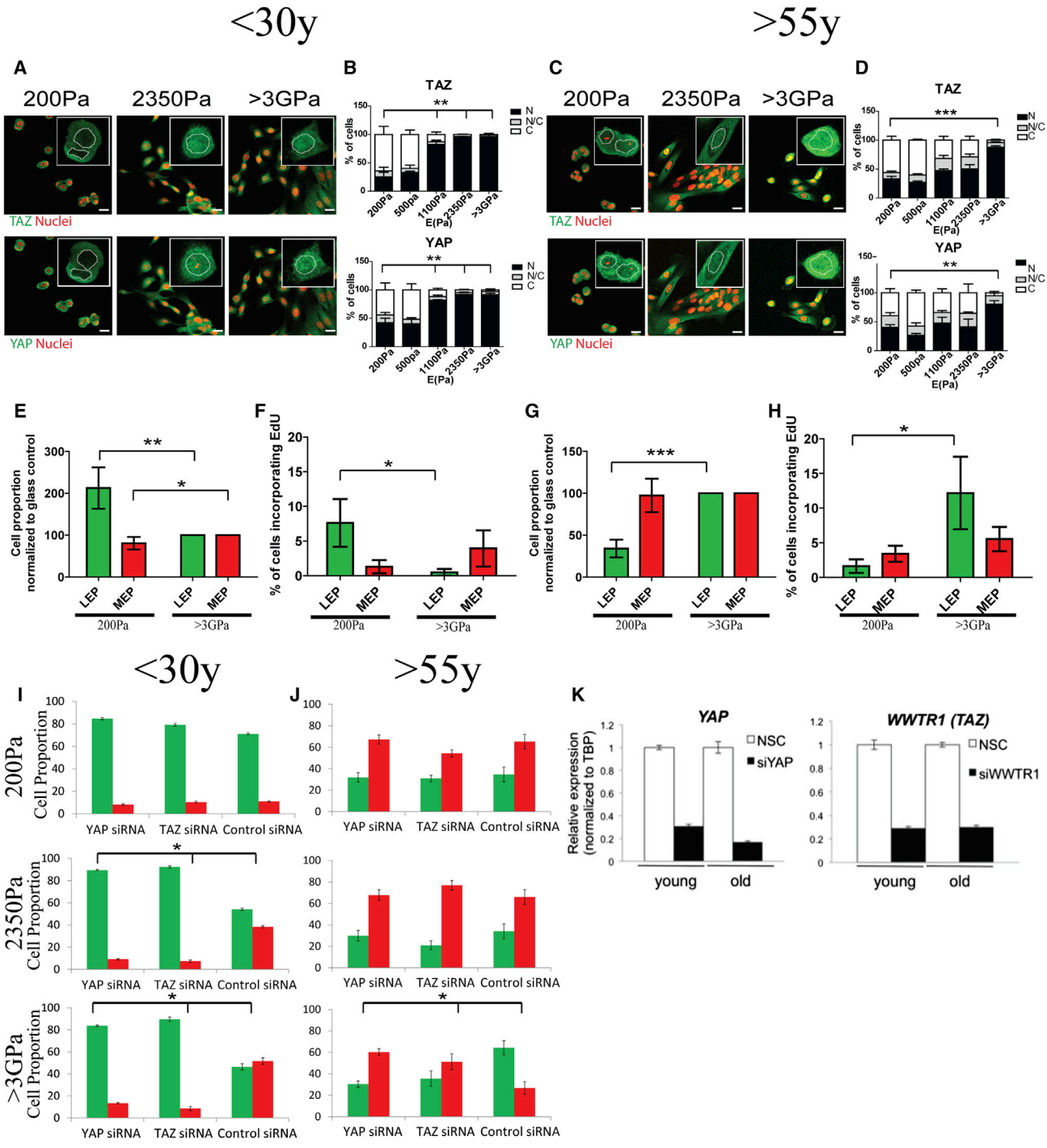

Figure 4. YAP and TAZ Activation Are Altered during Aging

(A and C) Representative IF images of TAZ, YAP (green), and DAPI (red) in cKit+ HMEC from (A) a young strain (240L; 19 years) and (C) an older strain (353P; 72 years). Bars represent 20 μm.

(B and D) Bar plots represent the distribution of YAP and TAZ (N, predominantly in the nucleus; N/C, equally distributed; C, predominantly in the cytoplasm) from over 100 cells/strain in (B) younger (n = 3) and (D) older (n = 3) strains.

(E and G) K19+LEP and K14+MEP proportions derived from cKit+ HMEC from (E) younger (n = 5) and (G) older (n = 5) women. Data are fold change of cell proportions compared to glass control ± SEM.

(F and H) Percentage of EdU$^+$ LEP and MEP derived from cKit+ HMEC from (F) younger (n = 5) and (H) older (n = 5) women. Data are means ± SEM.

(I and J) K19+LEP and K14+MEP proportions derived from cKit+ HMEC from (I) younger and (J) older strains transfected with YAP or TAZ siRNA.

(K) Bar graphs of YAP and TAZ transcript knockdown following siRNA treatment and NSC scrambled control siRNA.

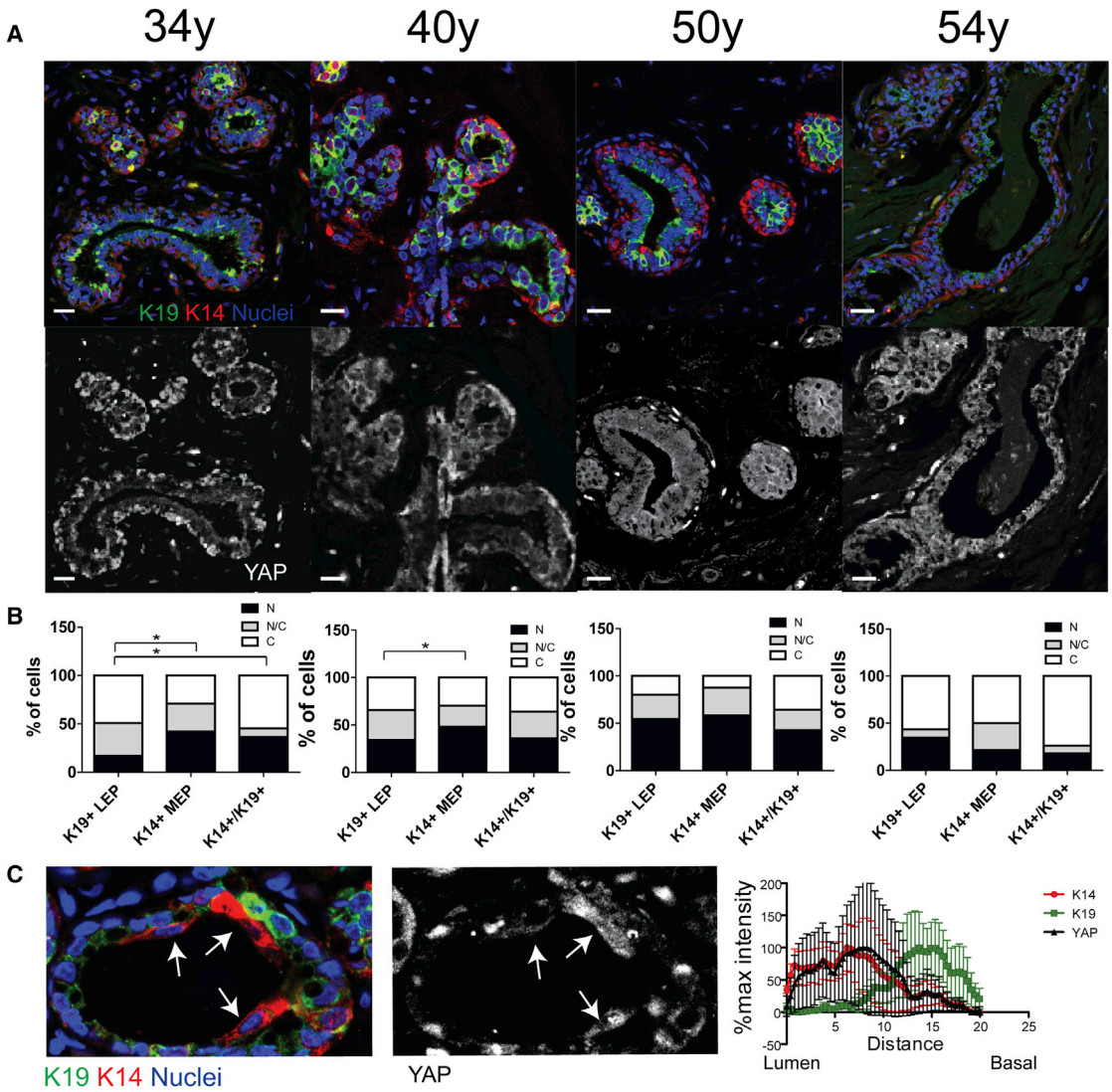

Figure 5. YAP Localization Changes with Age In Vivo

(A) Representative IF images of K14 (red), K19 (green), YAP (white), and DAPI (blue) in human mammary breast sections from four women (aged 34 years, 40 years, 50 years, and 54 years). Bars represent 20 μm.

(B) Bar plots represent the distribution of YAP (N, predominantly in the nucleus; N/C, equally distributed; C, predominantly in the cytoplasm) from over 100 cells/woman.

(C) YAP signal isolation from the immunofluorescence of K14 (red), K19 (green), YAP (white), and DAPI (blue) from the 34-year-old woman. Arrows identify luminal-positioned $K14^{+}/K19^{low/-}$ cells. The line graph shows mean pixel intensities from the lumen to the basal side of the structure in ten different examples of K14+ luminal cells.

See also Figure S6.

differences in Hippo gene expression were not strikingly age dependent in physiological conditions, we examined protein levels of MST1 and MST2. MST1 levels from three women <30 years and three women >55 years were not significantly different (Figures 6D–6G). MST2 protein levels were 3-fold greater in MPP from women >55 years compared to <30 years on 2,350 Pa gels (Figure 6E). Thus, it is tempting to speculate that age-dependent stoichiometry of Hippo pathway regulators can lead to insensitivity to mechanical cues and activation of YAP/TAZ.

Immortalization of Aged HMECs Restored Responsiveness to Physiological Stiffness

Cellular responses to mechanical stimuli are often examined with mesenchymal stem cells or immortal malignant and nonmalignant cell lines. Whereas immortal cell lines tend to proliferate more on stiffer substrata, we showed that normal <30 years HMEC exhibited lineage-dependent responses and that <55 years HMEC were nonresponsive to a physiological range of E (Figure 1). To better understand the differences between the normal and immortal nonmalignant states as a function of age,

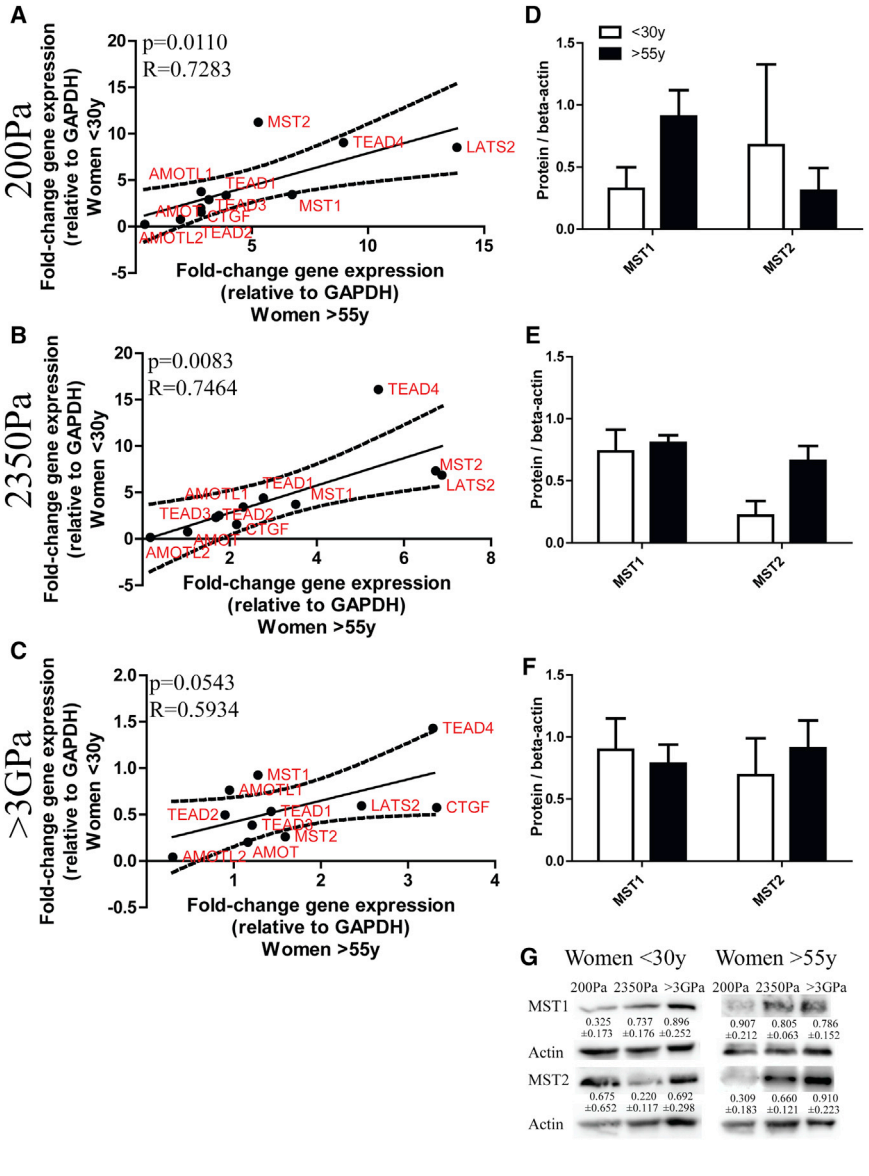

Figure 6. Age-Dependent Patterns of Hippo Pathway Components

(A–C) Correlation of gene expression between cKit+ HMEC from younger (n = 3) and older (n = 3) strains after 24 hr on (A) 200 Pa, (B) 2,350 Pa PA gels, and (C) >3 GPa substrate. Data are normalized to GAPDH expression.

(D–F) Western blot densitometric analysis of MST1 and MST2 from cKit+ HMEC from younger (n = 3) and older (n = 3) strains after 24 hr on (D) 200 Pa, (E) 2,350 Pa PA gels, and (F) >3 GPa substrate. Data are normalized to beta-actin protein content and are mean ± SEM.

(G) Representative western blot with quantification from a young (240L; 19 years) and an older strain (122L; 66 years).

we examined immortal nonmalignant cell lines derived from two young and two old primary HMEC strains by targeted inactivation of senescence barriers combined with unknown genomic errors (Stampfer et al., 2013). The cell lines, 240LMY (19 years), 184Fp16s (21 years), 122LMY (66 years), and 805Pp16s (91 years; Figure S7) were cultured atop PA gels tuned from 200 to 2,350 Pa. cKit+ MPP from 240LMY and 184Fp16s cell lines gave rise to more K14+ MEP than LEP on glass compared to 200 Pa PA gels (Figure 7A). cKit+ MPP from 122LMY and 805Pp16s gave rise to more K19+ LEP than MEP on glass compared to 200 Pa PA gels (Figure 7B). Independent of age, all lineages of the immortal cell lines incorporated more EdU as rigidity increased (Figures 7C–7F). YAP/TAZ nuclear translocation was detected both in <30 years and >55 years cell lines on PA gels from 200 to 2,350 Pa (Figures 7G–7N). Thus, immortalization of older HMEC restored sensitivity of the Hippo pathway to the physiological stiffness range, albeit abnormally because proliferation was no longer lineage-dependent. The propensity of immortal cell lines to generate more MEP or LEP on extraphysiological substrata was consistent with the chronological age of the HMEC, suggesting that the intrinsic age-related changes were stable.

DISCUSSION

Matrix rigidity is a determinant of mammary epithelial progenitor differentiation. Exposure of progenitors to mechanically tuned culture substrata revealed two fundamental changes that arise in MPP with age: (1) the mechanical trigger point for activation of YAP/TAZ increases, and (2) the YAP/TAZ-dependent differentiation programs become distinct. Culture of MPP from <30-year-old women in the most compliant 2D or 3D conditions (100–200 Pa) enhanced LEP differentiation, whereas stiffer substrata (2,300–3,800 Pa) favored MEP production. Older progenitors stochastically differentiated when exposed to a physiologically relevant elastic modulus range. Our results document the role of YAP/TAZ transcription factors as drivers of modulus-dependent differentiation in human mammary epithelial MPP and suggest that YAP/TAZ activity favors differentiation into MEP and other basal cell types. The basal cell types are not exclusive to MEP and may include LEP that express K14 or other basal-associated markers, which we and others have observed (Santagata et al., 2014). Older MPP needed to be stressed with extraphysiologically stiff substrata to reveal their YAP/TAZ-dependent bias toward LEP, which was consistent with our observation in vivo that YAP tended to be located in LEP with increased age. In younger women, YAP was in the nuclei of K14-expressing MEP, as well as the apical snouts of LEP. We previously demonstrated that postmenopausal LEP tend to express some K14, as well as other markers associated with MEP, and these new data suggest that

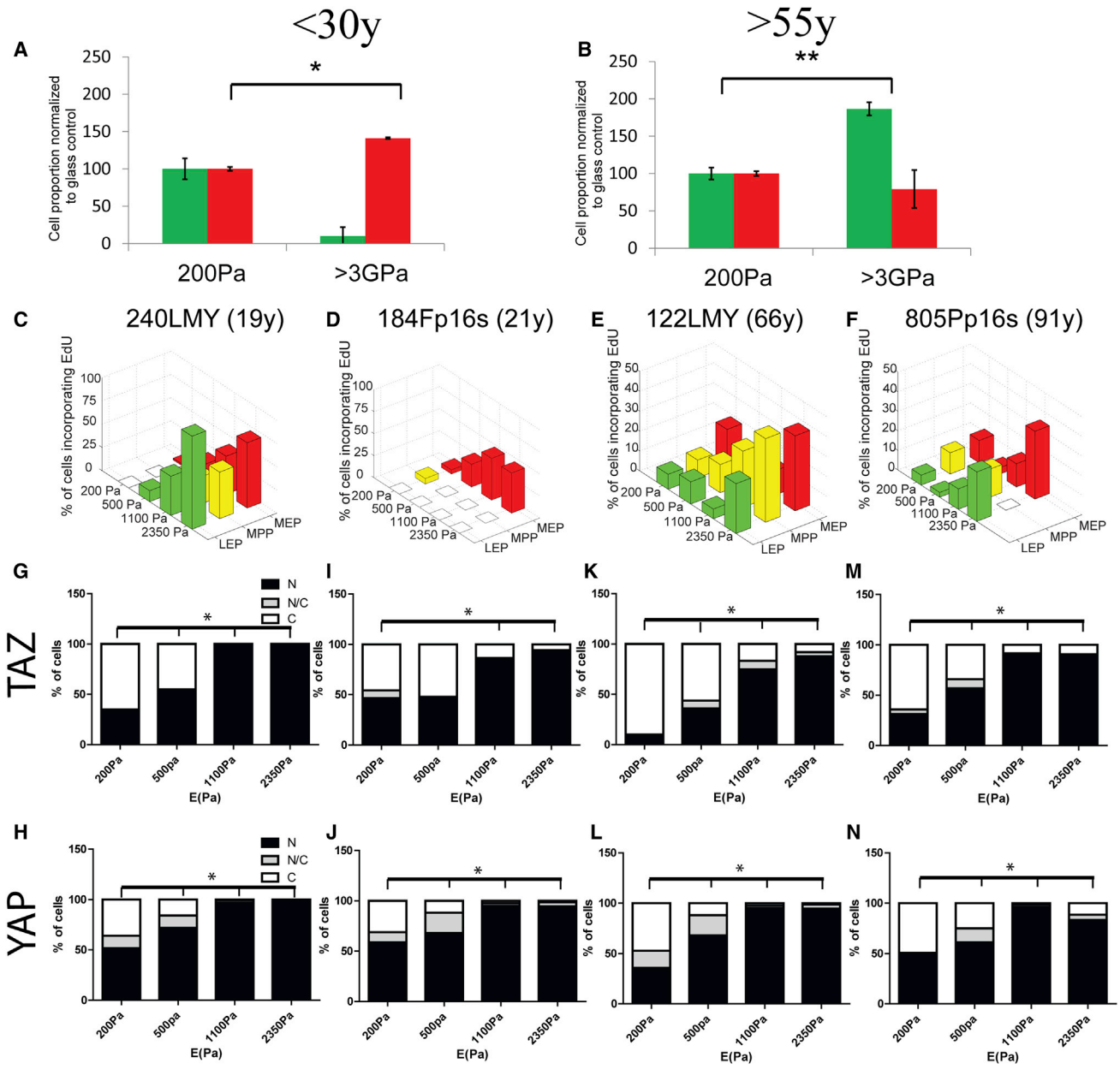

Figure 7. Immortalization Restores Responsiveness to Physiological Stiffness in Older HMEC

(A and B) K19+LEP and K14+MEP proportions derived from immortalized cell lines from (A) younger ($p = 0.0111$; $n = 2$ individuals in triplicate) and (B) older ($p = 0.0056$; $n = 2$ individuals in triplicate) women. Data are fold change of cell proportions compared to glass control ± SEM.

(C–F) Percentage of cells from immortalized cell lines derived from primary strains (240LMY at passage 25, 184Fp16s at passage 31, 122LMY at passage 19, and 805Pp16s at passage 29) incorporating EdU as a function of lineage, as defined by K14 and K19 expression, and stiffness.

(G–N) Bar plots represent the distribution of YAP and TAZ (N, predominantly in the nucleus; N/C, equally distributed; C, predominantly in the cytoplasm) from over 100 cells/lineage in immortalized cell lines. By comparison to the other cell lines, 184F derivatives are known to be mainly basal at the expense of LEP and progenitor phenotypes.

See also Figure S7.

age-dependent changes in YAP/TAZ activity may underlie that phenotype of aging.

Radiographic density of breast tissue tends to decrease with age suggesting that the mechanical environment is also altered (Benz, 2008), but mechanical forces do not exclusively govern YAP/TAZ regulation. Our experimental approach took advantage of tuned mechanical perturbations of matrix to functionally probe the HMEC, but more broadly these results revealed that aging fundamentally alters Hippo pathway regulation. The role of cell-cell contact in Hippo pathway regulation should be further

investigated in the context of chronological age. Both Wnt/beta-catenin and NF2 are known to regulate YAP/TAZ in vivo (Cockburn et al., 2013; Imajo et al., 2012), and changes to both pathways have been implicated in different age-related cancers (Evans et al., 2005; Seidler et al., 2004). Little is known about whether YAP/TAZ play a role in other phenotypes of aging. Deficiency in *C. elegans* yap-1 resulted in overall healthier aging relative to controls (Iwasa et al., 2013). Disrupted Hippo signaling in human and mouse ovarian follicles, which caused YAP activation, promoted growth and oocyte maturation, which are processes typically defective with age (Kawamura et al., 2013). Indirect evidence suggests mesenchymal stem cells also have dampened modulus-dependent differentiation responses with age. Bone is magnitudes stiffer than adipose tissue and the osteogenic potential of mesenchymal stem cells decreases and a bias toward adipogenesis increases with age (Moerman et al., 2004), but the role of Hippo is unclear.

Accumulation of MPP with age may be attributed to inefficient transduction of differentiation cues through the Hippo pathway. At low cell density, decreased Lats2 activity dependent on SF formation causes YAP/TAZ to translocate to the nucleus (Wada et al., 2011), but <30 years and >55 years MPP formed SF and FA comparably in response to changes in matrix stiffness. Thus, we explored the potential for stoichiometric imbalances in Hippo kinases with age that could dampen activation of YAP/TAZ. In our hands, MST2 protein was higher in >55 years MPP, suggestive of a damping mechanism. The Hippo pathway is implicated in differentiation of different progenitors into adipose, breast, muscle, and bone tissues, representing a wide range of elastic modulus and predicting a marvelously adaptable molecular rheostat. Each of these tissues differs in their matrix composition as well as physical attributes, and there is a reasonable expectation that combinations of ECM and growth factors tune Hippo pathway activity. Further study of microenvironment regulation of the Hippo pathway may identify components of the activation rheostat and reveal the basis for its age-related dampening.

Changes to the mechanical microenvironment affect multiple cell types in breast. High breast stiffness and density are correlated with increased risk and cancer progression (Yu et al., 2011). Increased stiffness also can induce adipocyte progenitors to differentiate into fibroblasts, which can positively feedback to further increase tissue stiffness (Chandler et al., 2012). MPP from women <30 years responded to increasingly rigid matrices by increased production of MEP, which are thought to be tumor suppressive (Gudjonsson et al., 2002; Hu et al., 2008), and proportionately decreased numbers of cells with the MPP phenotype, which are hypothesized to be breast cancer cells of origin (Lim et al., 2009), suggestive of a protective mechanism from tumor progression in younger epithelia. However, this putative protective mechanism falters with age, as demonstrated when aged HMEC were essentially unresponsive to physiological changes in matrix rigidity.

We speculate that the prevalence of luminal subtype breast cancers in postmenopausal women may be the result of age-acquired epigenetic states. When older MPP were exposed to extraphysiologically stiff substrata, they exhibited LEP-biased differentiation—the exact opposite of the younger progenitors. Age-dependent differentiation patterns were preserved in immortal young and old HMEC, but the mechanotransducive mechanism was notably rejuvenated in older immortal cells, enabling them to proliferate increasingly as matrix modulus approached that of a tumor. YAP/TAZ were required for shifting production in favor of MEP in younger and LEP in older MPP on the stiffer surfaces. We hypothesize that the distinct differentiation responses of younger and older MPP reflect age-dependent epigenetic landscapes. Indeed, normal HMEC exhibit age-dependent gene expression patterns consistent with the concept of age-dependent epigenetic states (Garbe et al., 2012). A precedent was set in hematopoietic stem cells where DNA and histone modifications were shown to correlate with age-related functional phenotypes (Chambers et al., 2007). Stromal feedback loops can result in formation of stiffened regions; if such regions already contained an accumulation of aged progenitor cells carrying errors predisposing them to immortality, they could create an environment that promotes development of age-related luminal subtype breast tumors.

Finally, it is important to be able to empirically examine the cell and molecular consequences of aging in normal human epithelia because most carcinomas are age-related. Wild-type mice are typically resistant to cancers, murine models of breast cancer do not completely model the steps of cancer progression in HMEC (Stampfer et al., 2013), and most inbred strains exhibit tumor incidence curves consistent with sporadic tumor genesis; thus, mice may not be an optimal model for studying the genesis of age-related breast cancers. Here, we present an approach for interrogation of human aging that takes advantage of cultured strains of normal HMEC and engineered microenvironments to perform cell-based molecular and functional studies, which are validated by comparison with breast tissues. Most studies that have drawn conclusions from breast cancer cell lines or mouse studies have used three methods to establish relevance of their results to human in vivo: an experiment with primary HMEC that recapitulates the main findings, examination of tissue sections for in vivo evidence that correlates with the findings, and correlation with large gene/protein expression data sets derived from patient samples. We have followed these three conventions. We find it striking that many of the molecular and biochemical phenotypes of aging persist in our early passage strains in spite of the imperfect microenvironment, which reinforces our impression that age-associated epigenetic changes are stabilizing those phenotypes. However, limitations and challenges are intrinsic to every experimental system. Early pregnancy has a detectable protective effect against breast cancer, and the balance of epithelial lineages and gene expression patterns in mice and humans are affected by parity (Choudhury et al., 2013). Our current strain collection is not annotated for parity information, and focused studies should be conducted to determine how parity modifies the aging phenotype in breast. There is an impressive level of heterogeneity among human mammary epithelia as was beautifully shown by detailed examinations of luminal lineages (Santagata et al., 2014; Shehata et al., 2012). Our method for establishing primary strains encompasses a significant amount of the total heterogeneity in given surgical specimen, and low stress culture conditions maintain MPP activity in early passages (Labarge et al., 2013).

Please cite this article in press as: Pelissier et al., Age-Related Dysfunction in Mechanotransduction Impairs Differentiation of Human Mammary Epithelial Progenitors, Cell Reports (2014), http://dx.doi.org/10.1016/j.celrep.2014.05.021

We also addressed this issue of heterogeneity and potential for interindividual variation by using strains established from 17 different women, with any given experiment comparing thousands of independent measurements from groups comprised of three to five strains each. We find repeatedly that the functional, molecular, and biochemical phenotypes often differ between the pre- and postmenopausal age groups, underscoring the importance of chronological age as an experimental variable.

EXPERIMENTAL PROCEDURES

Cell Culture

All cell culture was in M87A medium with cholera toxin at 0.5 ng/ml and oxytocin (X) at 0.1 nM (Bachem; Garbe et al., 2009). Primary HMEC strains were generated and maintained as described (Labarge et al., 2013); all tissues were obtained with proper oversight from the Lawrence Berkeley National Laboratory institutional review board. Modulus-dependent effects were measured in subconfluent cultures. Table S1 shows the strains used for each experiment.

Reagents

Cells were treated with Y27632 (10 μM; Sigma), ML-7 (10μM; Sigma), or calyculin A (2 nM; Calbiochem) 2 hr after adhesion. Cells were treated with PD98059 (50 μM; Cell Signaling Technology) 24 hr after adhesion. Cells were transfected with YAPsi, WWTR1 (TAZsi), or nontargeting control siRNA SMARTpools (Dharmacon/Thermo) plus a fluorescein isothiocyanate (FITC) label with DharmaFECT reagent according to manufacturer 24 hr prior to FACS enrichment.

Flow Cytometry

Anti-CD227-FITC (BD; clone HMPV; 1:50), anti-CD10-phycoerythrin (BioLegend; clone HI10a; 1:100), and anti-CD117-antigen-presenting cell (BioLegend; clone 104D2; 1:50) were added to cells in media for 25 min on ice, washed in PBS, and sorted with a FACSVantage DIVA (Becton Dickinson).

PA Gels

PA gels were made on circular, 12 mm coverslips etched in 0.1 M NaOH following an adapted protocol (Tse and Engler, 2010). Sulfo-SANPAH (0.4 mM) was activated by UV light, and then collagen was added (0.1 mg/ml in 50 mM HEPES; Sigma). ddH_2O washed gels were placed in polyHema-treated (0.133 ml at 12 mg/ml in 95% EtOH) 24-well plates. Gel modulus was confirmed with atomic force microscopy.

Immunofluorescence

HMEC were fixed in methanol:acetone (1:1) at −20°C for 15 min, blocked with PBS, 5% normal goat serum, 0.1% Triton X-100, and incubated with anti-K14 (1:1,000; Covance; polyclonal rabbit) and anti-K19 (1:20; Developmental Studies Hybridoma Bank; clone Troma-III) overnight at 4°C and then visualized with fluorescent secondary antibodies (Invitrogen) incubated for 2 hr at room temperature. EdU was added to culture media 4 hr prior to fixing cells and was imaged with Alexa 647 click reagents (Invitrogen). Paraformaldehyde (2.5%) was used for fixation for phalloidin (1:50; Invitrogen), anti-pFAK (1:1,000; Invitrogen; monoclonal antibody [mAb]), anti-vinculin (1:400; Sigma; mAb), anti-YAP (1:100; Santa Cruz Biotechnology; SC-15407), anti-TAZ (1:200; CST; polyclonal), phospho-p44/42 MAPK (Erk1/Erk2; 1:100; CST mAb), and p44/42 MAPK (Erk1/Erk2; 1:100; CST mAb). Paraformaldehyde (1.6%) was used for fixation for anti-CD227 (1:200; Abcam; polyclonal) and anti-CD10 (1:100; BD Biosciences; clone HI10a). Paraffin-embedded sections were deparaffinized and antigen retrieved (Vector Laboratories) and stained with primary antibodies to K14 (1:1,000; Covance; PRB-155P; visualized with A647 Zenon probes from Invitrogen), K19 (1:100; Abcam; AAH07628) and YAP (1:100; Santa Cruz; SC-15407). Cells were imaged with LSM710 confocal microscope (Carl Zeiss). Image analyses were conducted using a modified watershed method in Matlab software (Mathworks); see Supplemental Information for detailed code.

Real-Time PCR

Total RNA was purified with Trizol (Invitrogen) followed by RNeasy prep (QIAGEN). cDNA was synthesized with SuperScript III RT (Invitrogen). Transcripts levels were measured by qRT-PCR using iTaq SYBR Green Supermix (BioRad) and LightCycler480 (Roche). Primer sequences are in the Supplemental Information.

Generation of Immortal Cell Lines

Finite lifespan HMEC from specimens 184, 240L, 122L, and 805P were grown in M87A. Retroviral vectors: the p16 small hairpin RNA was in MSCV vector, and c-Myc was in pBabe–hygro (BH2) or LXSN vector. Retroviral stocks were generated from supernatants collected in M87A medium. Strains 240L, 122L, and 805P at passage 3 or and 184 at passage 4 were transduced with MSCV-p16sh or MSCV control and selected with puromycin. At the next passage, after puromycin selection, the p16sh-transduced cells were transduced with c-Myc pBabe–hygro (c-*myc* LXSN for 184) and selected with hygromycin. Vector-only control prestasis cells entered stasis at passages 12–15, whereas the immortalized lines continued to grow.

Western Blot

The following antibodies were used: MST1 CST no. 3682 rabbit 1:1,000, MST2 CST no. 3952 rabbit 1:1,000, beta-actin Abcam no. 8227 rabbit 1:500, and visualized with goat anti-rabbit immunoglobulin G (H + L)-horseradish peroxidase conjugate no. 170-6515 1:10,000.

TCGA Database

All data were obtained from the The Cancer Genome Atlas (TCGA) breast cancer online portal (https://tcga-data.nci.nih.gov/docs/publications/brca_2012/; Cancer Genome Atlas, 2012). The following files were used: for microarray gene expression data: "BRCA.exp.547.med.txt" and for reverse-phase protein array expression data: "rppaData-403Samp-171Ab-Trimmed.txt."

Statistical Analysis

Graphpad Prism 5.0 for PC and Matlab were used for all statistical analysis. Standard linear regression was used. Grouped analyses were performed with Bonferroni's test for multiple comparisons. To compare two population distributions, chi-square and t tests were performed. Significance was established when $*p < 0.05$, $**p < 0.01$, and $***p < 0.001$.

SUPPLEMENTAL INFORMATION

Supplemental Information includes Supplemental Experimental Procedures, seven figures, and two tables and can be found with this article at http://dx.doi.org/10.1016/j.celrep.2014.05.021.

AUTHOR CONTRIBUTIONS

F.A.P. and M.A.L. designed the research; F.A.P., J.C.G., B.A., M.M., C.L., T.J., J.B.L., and M.A.L. performed experiments; J.C.G., M.R.S., S.K., and M.A.L. provided cell strains and other key reagents; and F.A.P., J.B.L., and M.A.L. wrote the manuscript.

ACKNOWLEDGMENTS

We thank Prof. Matthias Lutolf, Gurkaran S. Buxi, and Thibault Vatter for expert advice. M.A.L. is supported by the NIH (NIA R00AG033176 and R01AG040081; NCI U54CA143836) and the US Department of Energy (DE-AC02-05CH11231). B.A. is supported by a postdoctoral fellowship from the California Institute for Regenerative Medicine (TG2-01164).

Received: March 20, 2013
Revised: April 15, 2014
Accepted: May 8, 2014
Published: June 5, 2014

REFERENCES

Ananthanarayanan, B., Kim, Y., and Kumar, S. (2011). Elucidating the mechanobiology of malignant brain tumors using a brain matrix-mimetic hyaluronic acid hydrogel platform. Biomaterials *32*, 7913–7923.

Beningo, K.A., Dembo, M., Kaverina, I., Small, J.V., and Wang, Y.L. (2001). Nascent focal adhesions are responsible for the generation of strong propulsive forces in migrating fibroblasts. J. Cell Biol. *153*, 881–888.

Benz, C.C. (2008). Impact of aging on the biology of breast cancer. Crit. Rev. Oncol. Hematol. *66*, 65–74.

Bershadsky, A.D., Balaban, N.Q., and Geiger, B. (2003). Adhesion-dependent cell mechanosensitivity. Annu. Rev. Cell Dev. Biol. *19*, 677–695.

Cancer Genome Atlas, N.; Cancer Genome Atlas Network (2012). Comprehensive molecular portraits of human breast tumours. Nature *490*, 61–70.

Chambers, S.M., Shaw, C.A., Gatza, C., Fisk, C.J., Donehower, L.A., and Goodell, M.A. (2007). Aging hematopoietic stem cells decline in function and exhibit epigenetic dysregulation. PLoS Biol. *5*, e201.

Chandler, E.M., Seo, B.R., Califano, J.P., Andresen Eguiluz, R.C., Lee, J.S., Yoon, C.J., Tims, D.T., Wang, J.X., Cheng, L., Mohanan, S., et al. (2012). Implanted adipose progenitor cells as physicochemical regulators of breast cancer. Proc. Natl. Acad. Sci. USA *109*, 9786–9791.

Charruyer, A., Barland, C.O., Yue, L., Wessendorf, H.B., Lu, Y., Lawrence, H.J., Mancianti, M.L., and Ghadially, R. (2009). Transit-amplifying cell frequency and cell cycle kinetics are altered in aged epidermis. J. Invest. Dermatol. *129*, 2574–2583.

Cho, R.H., Sieburg, H.B., and Muller-Sieburg, C.E. (2008). A new mechanism for the aging of hematopoietic stem cells: aging changes the clonal composition of the stem cell compartment but not individual stem cells. Blood *111*, 5553–5561.

Choudhury, S., Almendro, V., Merino, V.F., Wu, Z., Maruyama, R., Su, Y., Martins, F.C., Fackler, M.J., Bessarabova, M., Kowalczyk, A., et al. (2013). Molecular profiling of human mammary gland links breast cancer risk to a p27(+) cell population with progenitor characteristics. Cell Stem Cell *13*, 117–130.

Cockburn, K., Biechele, S., Garner, J., and Rossant, J. (2013). The Hippo pathway member Nf2 is required for inner cell mass specification. Curr. Biol. *23*, 1195–1201.

Dupont, S., Morsut, L., Aragona, M., Enzo, E., Giulitti, S., Cordenonsi, M., Zanconato, F., Le Digabel, J., Forcato, M., Bicciato, S., et al. (2011). Role of YAP/TAZ in mechanotransduction. Nature *474*, 179–183.

Engler, A.J., Sen, S., Sweeney, H.L., and Discher, D.E. (2006). Matrix elasticity directs stem cell lineage specification. Cell *126*, 677–689.

Evans, D.G., Maher, E.R., and Baser, M.E. (2005). Age related shift in the mutation spectra of germline and somatic NF2 mutations: hypothetical role of DNA repair mechanisms. J. Med. Genet. *42*, 630–632.

Garbe, J.C., Bhattacharya, S., Merchant, B., Bassett, E., Swisshelm, K., Feiler, H.S., Wyrobek, A.J., and Stampfer, M.R. (2009). Molecular distinctions between stasis and telomere attrition senescence barriers shown by long-term culture of normal human mammary epithelial cells. Cancer Res. *69*, 7557–7568.

Garbe, J.C., Pepin, F., Pelissier, F.A., Sputova, K., Fridriksdottir, A.J., Guo, D.E., Villadsen, R., Park, M., Petersen, O.W., Borowsky, A.D., et al. (2012). Accumulation of multipotent progenitors with a basal differentiation bias during aging of human mammary epithelia. Cancer Res. *72*, 3687–3701.

Gudjonsson, T., Rønnov-Jessen, L., Villadsen, R., Rank, F., Bissell, M.J., and Petersen, O.W. (2002). Normal and tumor-derived myoepithelial cells differ in their ability to interact with luminal breast epithelial cells for polarity and basement membrane deposition. J. Cell Sci. *115*, 39–50.

Halder, G., Dupont, S., and Piccolo, S. (2012). Transduction of mechanical and cytoskeletal cues by YAP and TAZ. Nat. Rev. Mol. Cell Biol. *13*, 591–600.

Haralick, R.M., Shanmugam, K., and Dinstein, I. (1973). Textural features for image classification. IEEE Trans. Syst. Man Cyb. *SMC-3*, 610–621.

Henry, C.J., Marusyk, A., and DeGregori, J. (2011). Aging-associated changes in hematopoiesis and leukemogenesis: what's the connection? Aging (Albany, N.Y. Online) *3*, 643–656.

Hu, M., Yao, J., Carroll, D.K., Weremowicz, S., Chen, H., Carrasco, D., Richardson, A., Violette, S., Nikolskaya, T., Nikolsky, Y., et al. (2008). Regulation of in situ to invasive breast carcinoma transition. Cancer Cell *13*, 394–406.

Imajo, M., Miyatake, K., Iimura, A., Miyamoto, A., and Nishida, E. (2012). A molecular mechanism that links Hippo signalling to the inhibition of Wnt/β-catenin signalling. EMBO J. *31*, 1109–1122.

Ishizaki, T., Naito, M., Fujisawa, K., Maekawa, M., Watanabe, N., Saito, Y., and Narumiya, S. (1997). p160ROCK, a Rho-associated coiled-coil forming protein kinase, works downstream of Rho and induces focal adhesions. FEBS Lett. *404*, 118–124.

Iwasa, H., Maimaiti, S., Kuroyanagi, H., Kawano, S., Inami, K., Timalsina, S., Ikeda, M., Nakagawa, K., and Hata, Y. (2013). Yes-associated protein homolog, YAP-1, is involved in the thermotolerance and aging in the nematode Caenorhabditis elegans. Exp. Cell Res. *319*, 931–945.

Kanai, F., Marignani, P.A., Sarbassova, D., Yagi, R., Hall, R.A., Donowitz, M., Hisaminato, A., Fujiwara, T., Ito, Y., Cantley, L.C., and Yaffe, M.B. (2000). TAZ: a novel transcriptional co-activator regulated by interactions with 14-3-3 and PDZ domain proteins. EMBO J. *19*, 6778–6791.

Kawamura, K., Cheng, Y., Suzuki, N., Deguchi, M., Sato, Y., Takae, S., Ho, C.H., Kawamura, N., Tamura, M., Hashimoto, S., et al. (2013). Hippo signaling disruption and Akt stimulation of ovarian follicles for infertility treatment. Proc. Natl. Acad. Sci. USA *110*, 17474–17479.

Kimura, K., Ito, M., Amano, M., Chihara, K., Fukata, Y., Nakafuku, M., Yamamori, B., Feng, J., Nakano, T., Okawa, K., et al. (1996). Regulation of myosin phosphatase by Rho and Rho-associated kinase (Rho-kinase). Science *273*, 245–248.

Knoth, R., Singec, I., Ditter, M., Pantazis, G., Capetian, P., Meyer, R.P., Horvat, V., Volk, B., and Kempermann, G. (2010). Murine features of neurogenesis in the human hippocampus across the lifespan from 0 to 100 years. PLoS ONE *5*, e8809.

Kuranda, K., Vargaftig, J., de la Rochere, P., Dosquet, C., Charron, D., Bardin, F., Tonnelle, C., Bonnet, D., and Goodhardt, M. (2011). Age-related changes in human hematopoietic stem/progenitor cells. Aging Cell *10*, 542–546.

LaBarge, M.A., Nelson, C.M., Villadsen, R., Fridriksdottir, A., Ruth, J.R., Stampfer, M.R., Petersen, O.W., and Bissell, M.J. (2009). Human mammary progenitor cell fate decisions are products of interactions with combinatorial microenvironments. Integr. Biol. (Camb.) *1*, 70–79.

Labarge, M.A., Garbe, J.C., and Stampfer, M.R. (2013). Processing of human reduction mammoplasty and mastectomy tissues for cell culture. J. Vis. Exp. (71), pii: 50011.

Lim, E., Vaillant, F., Wu, D., Forrest, N.C., Pal, B., Hart, A.H., Asselin-Labat, M.L., Gyorki, D.E., Ward, T., Partanen, A., et al.; kConFab (2009). Aberrant luminal progenitors as the candidate target population for basal tumor development in BRCA1 mutation carriers. Nat. Med. *15*, 907–913.

Lui, C., Lee, K., and Nelson, C.M. (2012). Matrix compliance and RhoA direct the differentiation of mammary progenitor cells. Biomech. Model. Mechanobiol. *11*, 1241–1249.

Moerman, E.J., Teng, K., Lipschitz, D.A., and Lecka-Czernik, B. (2004). Aging activates adipogenic and suppresses osteogenic programs in mesenchymal marrow stroma/stem cells: the role of PPAR-gamma2 transcription factor and TGF-beta/BMP signaling pathways. Aging Cell *3*, 379–389.

Nguyen, L.V., Makarem, M., Carles, A., Moksa, M., Kannan, N., Pandoh, P., Eirew, P., Osako, T., Kardel, M., Cheung, A.M., et al. (2014). Clonal analysis via barcoding reveals diverse growth and differentiation of transplanted mouse and human mammary stem cells. Cell Stem Cell *14*, 253–263.

Pang, W.W., Price, E.A., Sahoo, D., Beerman, I., Maloney, W.J., Rossi, D.J., Schrier, S.L., and Weissman, I.L. (2011). Human bone marrow hematopoietic stem cells are increased in frequency and myeloid-biased with age. Proc. Natl. Acad. Sci. USA *108*, 20012–20017.

Please cite this article in press as: Pelissier et al., Age-Related Dysfunction in Mechanotransduction Impairs Differentiation of Human Mammary Epithelial Progenitors, Cell Reports (2014), http://dx.doi.org/10.1016/j.celrep.2014.05.021

Pantic, I., Pantic, S., and Basta-Jovanovic, G. (2012). Gray level co-occurrence matrix texture analysis of germinal center light zone lymphocyte nuclei: physiology viewpoint with focus on apoptosis. Microsc. Microanal. *18*, 470–475.

Paszek, M.J., Zahir, N., Johnson, K.R., Lakins, J.N., Rozenberg, G.I., Gefen, A., Reinhart-King, C.A., Margulies, S.S., Dembo, M., Boettiger, D., et al. (2005). Tensional homeostasis and the malignant phenotype. Cancer Cell *8*, 241–254.

Provenzano, P.P., Inman, D.R., Eliceiri, K.W., and Keely, P.J. (2009). Matrix density-induced mechanoregulation of breast cell phenotype, signaling and gene expression through a FAK-ERK linkage. Oncogene *28*, 4326–4343.

Rios, A.C., Fu, N.Y., Lindeman, G.J., and Visvader, J.E. (2014). In situ identification of bipotent stem cells in the mammary gland. Nature *506*, 322–327.

Santagata, S., Thakkar, A., Ergonul, A., Wang, B., Woo, T., Hu, R., Harrell, J.C., McNamara, G., Schwede, M., Culhane, A.C., et al. (2014). Taxonomy of breast cancer based on normal cell phenotype predicts outcome. J. Clin. Invest. *124*, 859–870.

Seidler, H.B., Utsuyama, M., Nagaoka, S., Takemura, T., Kitagawa, M., and Hirokawa, K. (2004). Expression level of Wnt signaling components possibly influences the biological behavior of colorectal cancer in different age groups. Exp. Mol. Pathol. *76*, 224–233.

Shehata, M., Teschendorff, A., Sharp, G., Novcic, N., Russell, A., Avril, S., Prater, M., Eirew, P., Caldas, C., Watson, C.J., and Stingl, J. (2012). Phenotypic and functional characterization of the luminal cell hierarchy of the mammary gland. Breast Cancer Res. *14*, R134.

Stampfer, M.M., LaBarge, M.A., and Garbe, J.C. (2013). An Integrated Human Mammary Epithelial Cell Culture System for Studying Carcinogenesis and Aging. In Cell and Molecular Biology of Breast Cancer, H. Schatten, ed. (New York: Springer), pp. 323–361.

Stoll, E.A., Habibi, B.A., Mikheev, A.M., Lasiene, J., Massey, S.C., Swanson, K.R., Rostomily, R.C., and Horner, P.J. (2011). Increased re-entry into cell cycle mitigates age-related neurogenic decline in the murine subventricular zone. Stem Cells *29*, 2005–2017.

Tamada, M., Sheetz, M.P., and Sawada, Y. (2004). Activation of a signaling cascade by cytoskeleton stretch. Dev. Cell *7*, 709–718.

Tse, J.R., and Engler, A.J. (2010). Preparation of hydrogel substrates with tunable mechanical properties. Curr. Protoc. Cell Biol. *Chapter 10*, Unit 10.16.

Villadsen, R., Fridriksdottir, A.J., Rønnov-Jessen, L., Gudjonsson, T., Rank, F., LaBarge, M.A., Bissell, M.J., and Petersen, O.W. (2007). Evidence for a stem cell hierarchy in the adult human breast. J. Cell Biol. *177*, 87–101.

Vogel, V., and Sheetz, M. (2006). Local force and geometry sensing regulate cell functions. Nat. Rev. Mol. Cell Biol. *7*, 265–275.

Wada, K., Itoga, K., Okano, T., Yonemura, S., and Sasaki, H. (2011). Hippo pathway regulation by cell morphology and stress fibers. Development *138*, 3907–3914.

Yu, H., Mouw, J.K., and Weaver, V.M. (2011). Forcing form and function: biomechanical regulation of tumor evolution. Trends Cell Biol. *21*, 47–56.

Zhao, B., Wei, X., Li, W., Udan, R.S., Yang, Q., Kim, J., Xie, J., Ikenoue, T., Yu, J., Li, L., et al. (2007). Inactivation of YAP oncoprotein by the Hippo pathway is involved in cell contact inhibition and tissue growth control. Genes Dev. *21*, 2747–2761.

Zhao, B., Li, L., Lu, Q., Wang, L.H., Liu, C.Y., Lei, Q., and Guan, K.L. (2011). Angiomotin is a novel Hippo pathway component that inhibits YAP oncoprotein. Genes Dev. *25*, 51–63.

Supplemental Table S1, related to Experimental Procedures: Primary cell strains and immortal cell lines

Figure		1	1	1	2	3	4	4	4	5	6	6	7	S4	S5
Strain	**Age (years)**	**A-D' I, J**	**E-H**	**K-N'**			**A-D**	**E-H**	**I-K**		**A-C**	**D-G**			
160	**16**			1p	4p	4p									
240L	**19**	4p	4p		4p	4p	4p	4p	4p *		4p	4p		4p	4p
168R	**19**	4p	4p		4p	4p	4p	4p			4p	4p		4p	4p
53R	**19**			1p											
184	**21**	4p						4p			4p			4p	
51R	**27**			1p											
123	**27**	4p						4p			4p			4p	
124	**29**	4p	4p					4p			4p	4p		4p	4p
1030P	**30**						4p								
BR048	**34**									0p					
BR038	**40**									0p					
BR039	**50**									0p					
BR040	**54**									0p					
96L	**61**			1p											
71C	**65**			1p											
881P	**65**	4p						4p			4p			4p	
122L	**66**	4p	4p		4p	4p	4p	4p	4p *		4p	4p		4p	4p
29	**68**		4p	1p								4p			4p
429ER	**72**				4p	4p									
353P	**72**	4p	4p				4p	4p			4p	4p		4p	4p
464P	**80**	4p			4p	4p	4p	4p			4p			4p	
451P	**83**	4p						4p			4p			4p	
Immortal cell lines															
240LMY	**19**												25p		
184Fp16s	**21**												31p		
122LMY	**66**												19p		
805Pp16s	**91**												29p		

*: Technical triplicates p: Passage

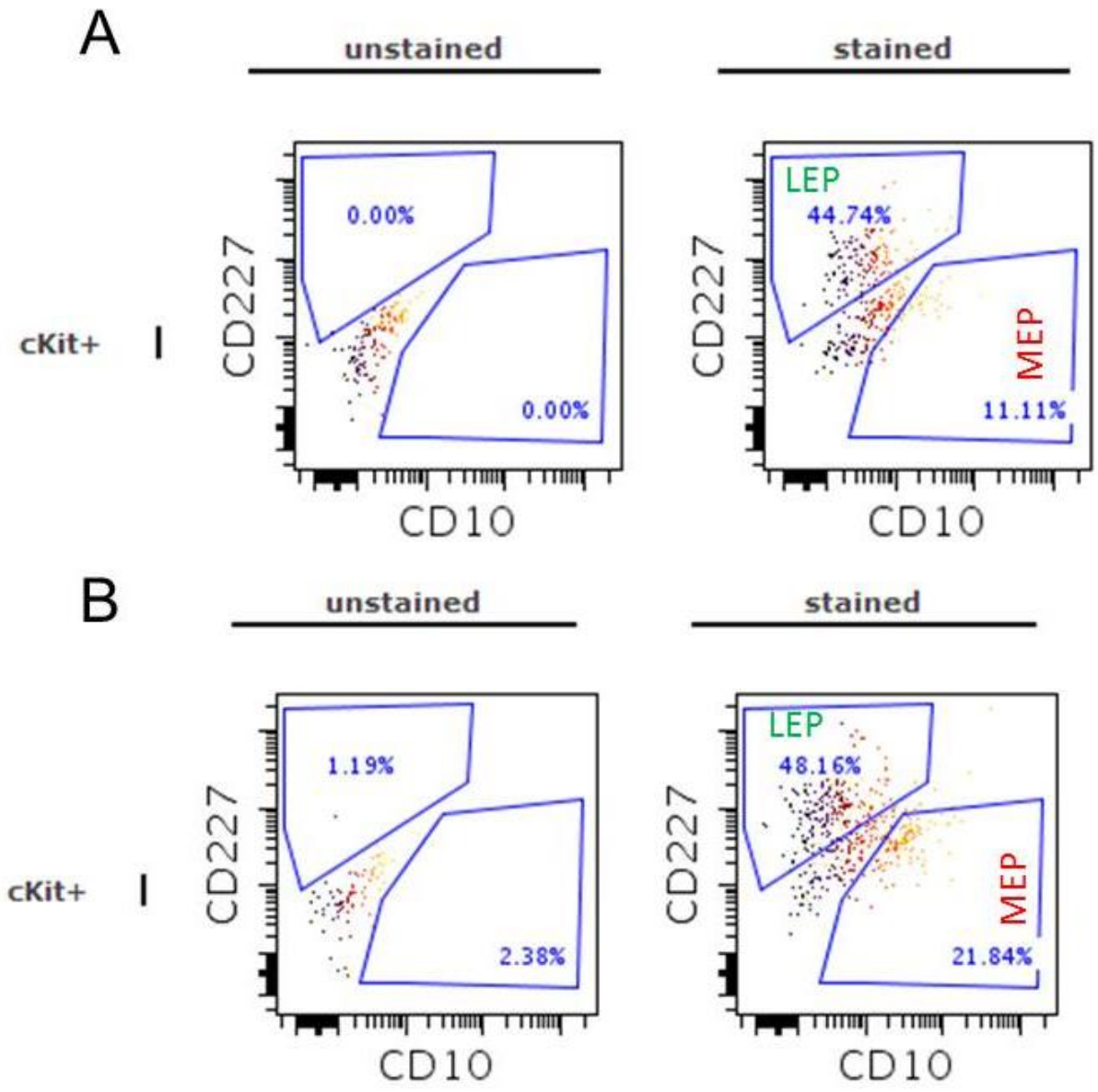

Figure S1, related to Experimental Procedures. (A) Representative FACS analyses showing CD227 and CD10 expression in fourth-passage cKit-enriched HMEC isolated from one woman younger than 30 years (160 16y) and (B) one older than 55 years (429ER 72y). Left, unstained controls; right, the CD10- and CD227-stained samples.

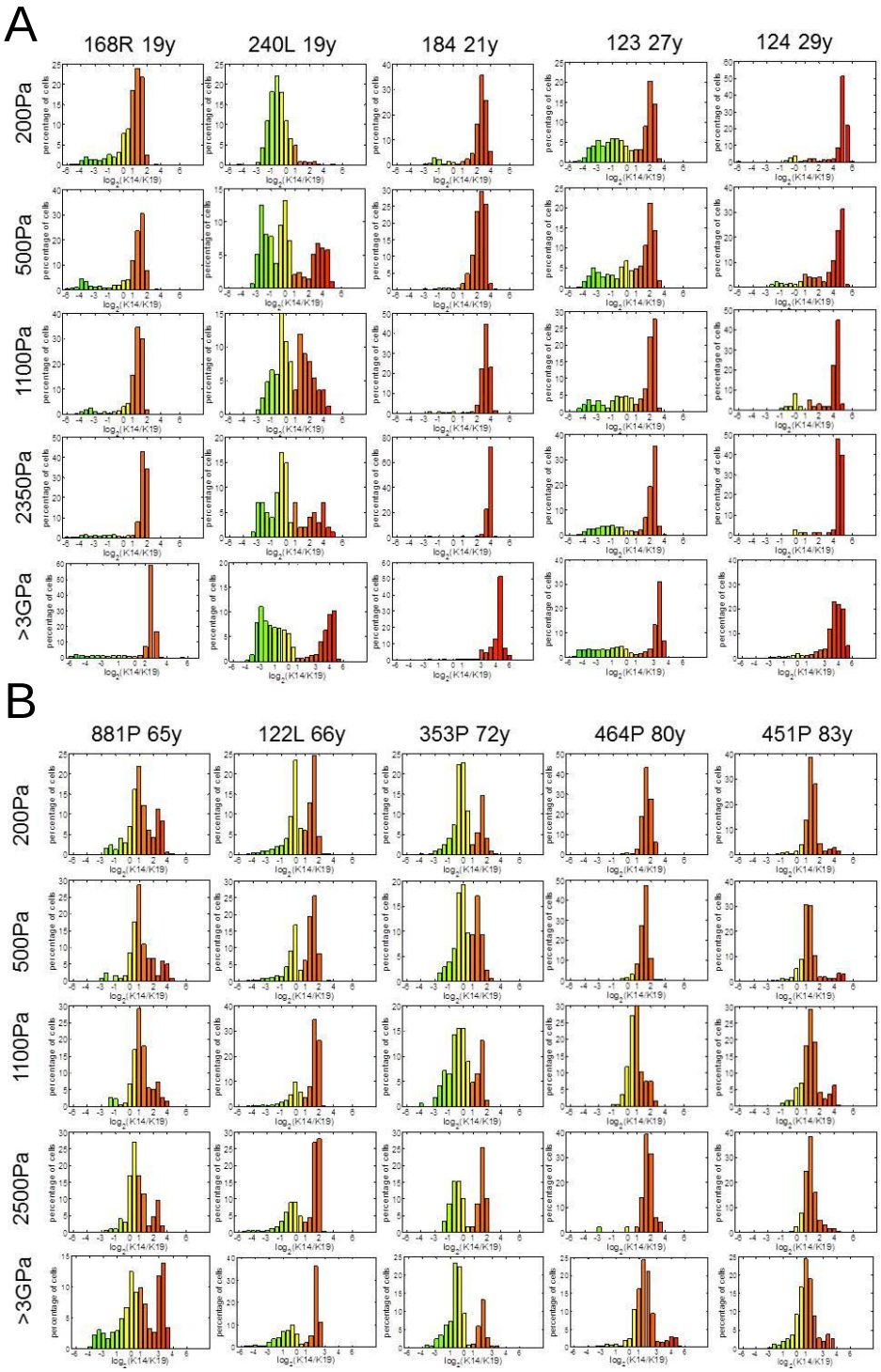

Figure S2, related to Figure 1 (A) Histograms represent log_2-transformed ratios of K14 to K19 protein expression in single cells for each donor <30y under each condition. (B) Histograms represent log_2-transformed ratios of K14 to K19 protein expression in single cells for each donor >55y under each condition.

Supplemental Table S2 related to Figure S2: p-values obtained with a Chi-squared test.

Conditions	Strain	168R	240L	184	123	124	881P	122L	353P	464P	451P
200Pa vs 500Pa		0.127	0.000	0.688	0.846	0.008	0.492	0.202	0.357	0.417	0.281
200Pa vs 1100Pa		0.054	0.003	0.010	0.096	0.000	0.459	0.235	0.162	0.166	0.124
200Pa vs 2350Pa		0.001	0.036	0.001	0.007	0.013	0.053	0.051	0.054	0.392	0.522
200Pa vs >3GPa		0.003	0.000	0.044	0.039	0.000	0.035	0.002	0.001	0.023	0.000

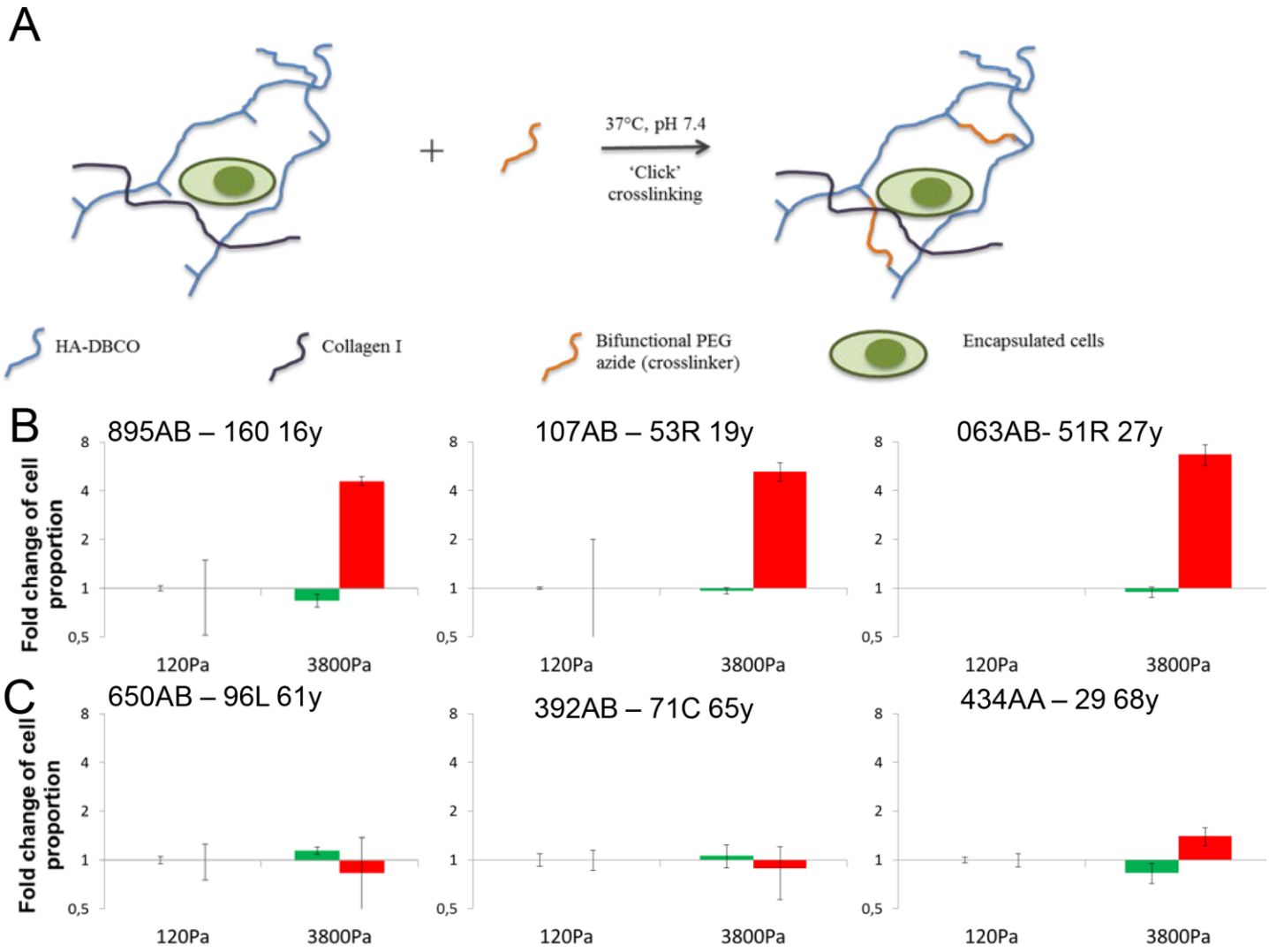

Figure S3, related to Figure 1. (A) Cartoon schematic of 3D encapsulation in click-crosslinked hyaluronic acid (HA) hydrogels. Fold change of lineage proportions in passage 1 cKit+ HMEC from donors (B) <30y and (C) >55y in HA gels with increasing stiffness.

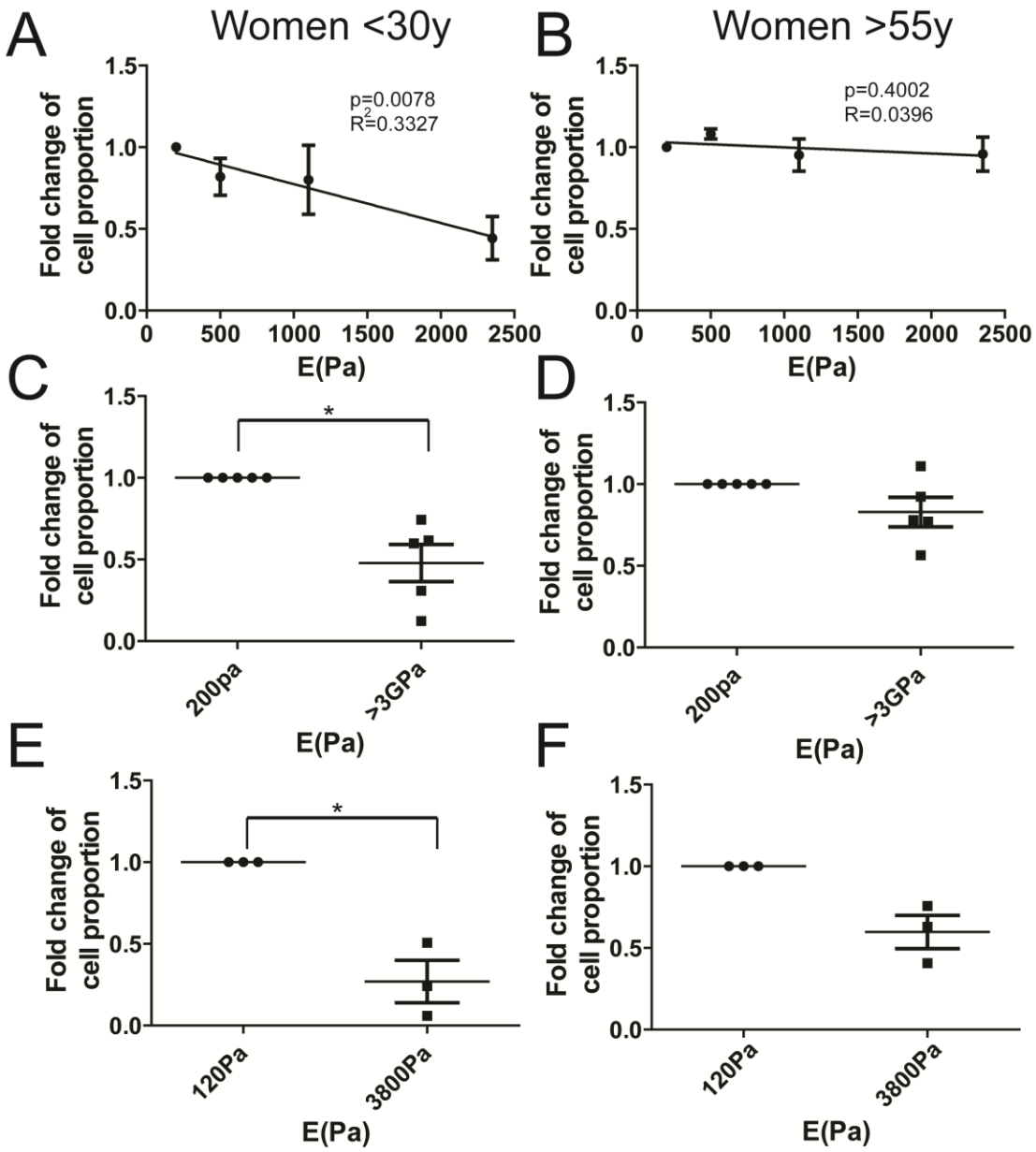

Figure S4, related to Figure 1. (A) Linear regression plots of K14+/K19+ HMEC proportion as a function of modulus are shown for women <30y (p=0.0078, r^2= 0.3327, n=5) and (B) women >55 (p=0.4002, r^2= 0.0396, n=5). (C) K14+/K19+ HMEC proportion as a function of modulus is shown for women <30y (p=0.0101, n=5) and (D) women >55 (p=0.0577, n=5). Regressions and plots are fold change of proportions compared to 200Pa condition ± s.e.m. (E) Fold changes of K14+/K19+ HMEC proportion normal to 120Pa condition after 7 days of culture encapsulated in 3D hyaluronic acid (HA) gels (women <30y p=0.0301, n=3, F, women >55y p=0.0587).

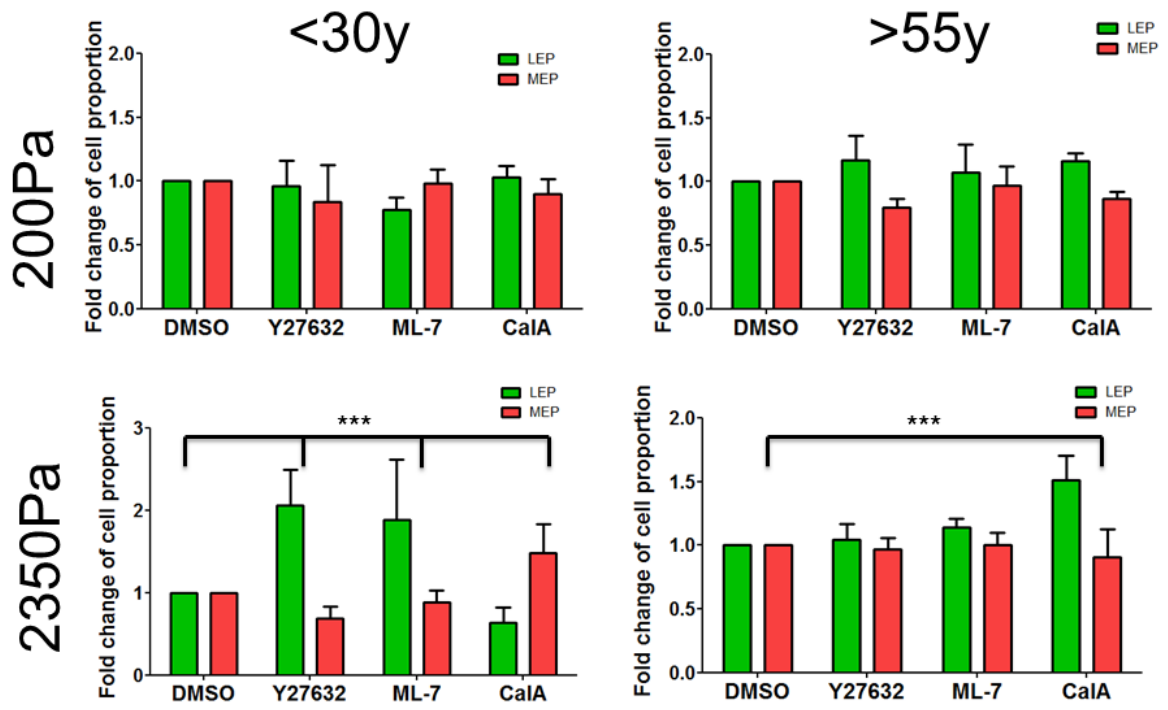

Figure S5, related to Figure 3. Fold change of lineage proportions in cKit+ HMEC from women <30y and >55y on 200Pa and 2350Pa PA gels treated with mechano-sensing inhibitors.

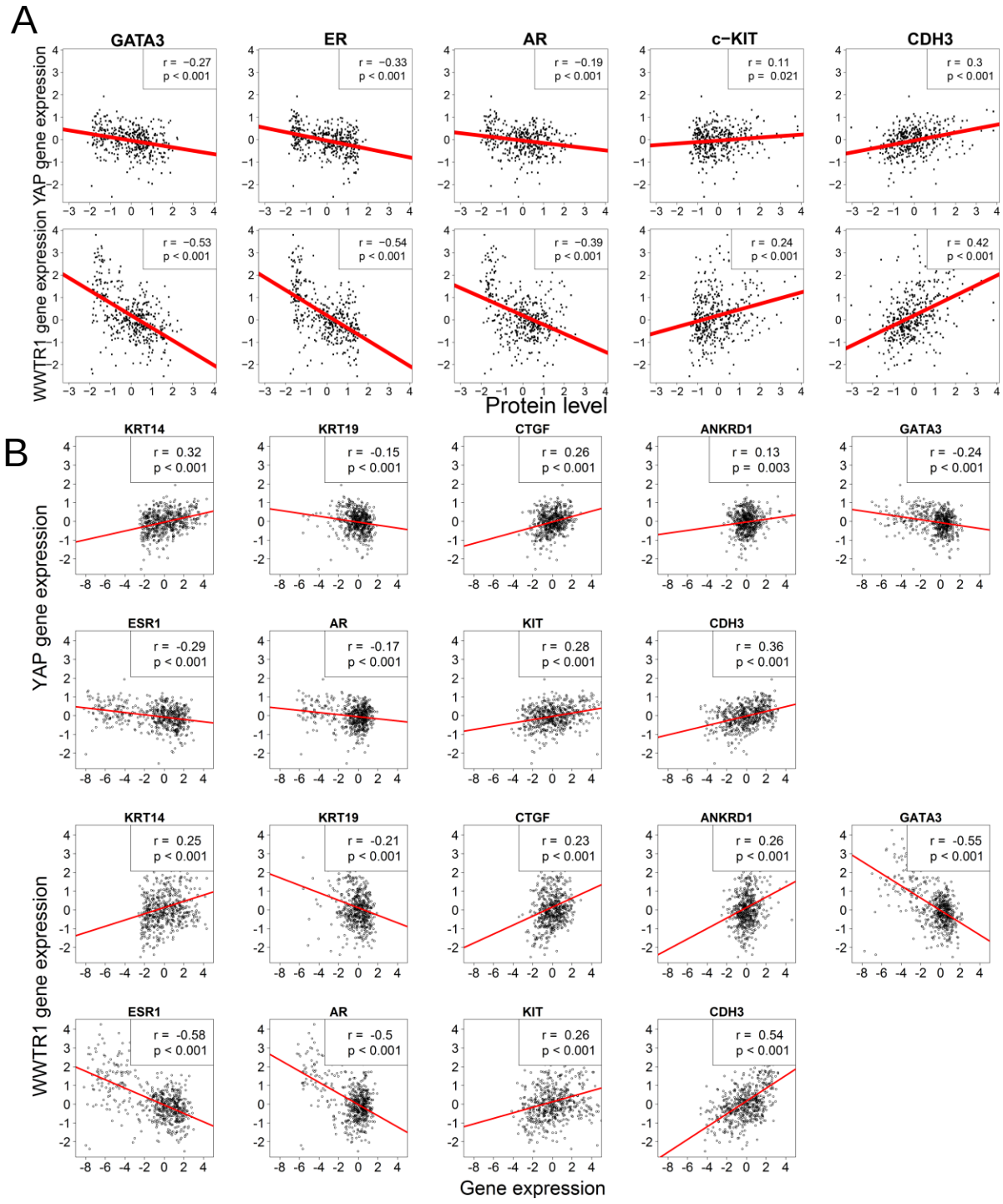

Figure S6 related to Figure 5. (A) Correlation between YAP and TAZ gene expression and the protein expression of various biomarkers in TCGA dataset (Pearson's r statistic is shown). (B) Correlation between YAP and TAZ gene expression and various biomarkers gene expression from the TCGA dataset.

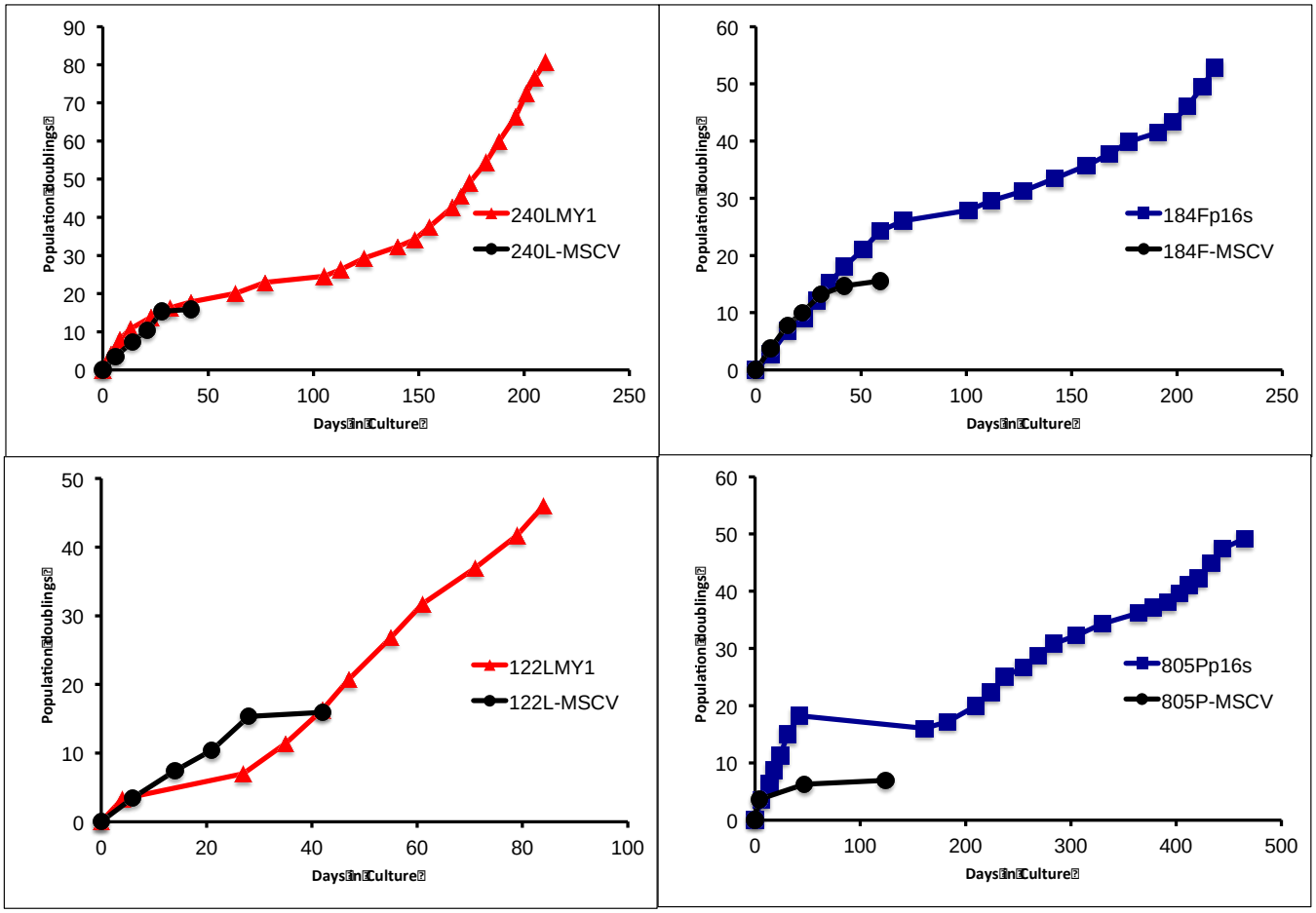

Figure S7, related to Figure 7. Growth curves for the four immortal lines used and the MSCV-vector only controls that entered stasis.

Supplemental Experimental Procedures:

Primers used for qRT-PCR:

The primer sets were designed to target two different exons of the gene.

GAPDH	AAGGTGAAGGTCGGAGTCAAC,	GGGGTCATTGATGGCAACAATA
TEAD1	GGCCGGGAATGATTCAAACAG,	CAATGGAGCGACCTTGCCA
TEAD2	GCCTCCGAGAGCTATATGATCG,	TCACTCCGTAGAAGCCACCA
TEAD3	TCATCCACAAGCTGAAGCAC,	CAATGACAAGCAGGGTCTCC
TEAD4	GGACATCCGCCAAATCTATG,	TCCTCGATGTTGGTGTTGAG
MST1	CCTCCCACATTCCGAAAACCA,	GCACTCCTGACAAATGGGTG
MST2	AGGAACAGCAACGAGAATTGG,	CCCCTTCACTCATCGTGCTT
LATS2	CAGCTGGAGCAAGAAATGG,	TGGCCCTCTTTAACCTGTTG
AMOT	AGGCAAGAGTTGGAAGGATG,	TTGGAGGATGACTTCACGAG
AMOTL1	TGCATGTGAGAAGCGAGAAC,	CATTGTATTCCGGCATGTTG
AMOTL2	ACCATGCGGAACAAGATGGAC,	GGCGGCGATTTGCAGATTC
CTGF	CGGGTTACCAATGACAACG,	TGGAGATTTTGGGAGTACGG

3D encapsulation in Hyaluronic Acid (HA) gels - Passage 1 cKit+ HMEC were encapsulated in click-crosslinked HA hydrogels (Figure S3A). Details will be published elsewhere, but briefly**,** HA-dibenzocyclooctyne (HA-DBCO) was synthesized as follows: HA-COOH (65 kDa molecular weight, Lifecore Biomedical) was dissolved in water, activated by EDC/NHS (N-(3-Dimethylaminopropyl)-N′-ethylcarbodiimide/N-hydroxysuccinimide, Sigma-Aldrich) and reacted with DBCO-amine (Sigma-Aldrich) dissolved in dimethyl sulfoxide for 48h at room temperature, followed by dialysis and freeze-drying to obtain HA-DBCO with approximately 10% of the HA disaccharide units modified by DBCO (from ^{1}H NMR data, not shown). HA-DBCO was crosslinked by ‘click’ chemistry using bifunctional PEG-azide (1 kDa molecular weight, Creative Pegworks) to form hydrogels rapidly via the Strain-Promoted Azide-Alkyne Cycloaddition (SPAAC) reaction (Ning, Guo et al. 2008). The elastic modulus of the hydrogels was modified similar to that described previously (Ananthanarayanan, Kim et al. 2011) by

varying HA content and the ratio (r) of azide groups to HA disaccharide units. The two formulations chosen were 1.5 wt% HA, r = 0.15 and 3 wt% HA, r = 0.09, corresponding to Young's moduli of 123 ± 37 Pa and 3843 ± 306 Pa respectively as measured by oscillatory shear rheology. For 3D cell encapsulation, hydrogels were prepared on glass chamber-slides treated with a hydrophobic solution. HA-DBCO was mixed with Collagen I (PureCol bovine collagen, Advanced Biomatrix) to 0.03 wt%. PEG-azide was added just prior to mixing with the cell pellet, and the solution was allowed to gel for 1h at 37 °C before adding media. Cell-gel constructs were maintained for 7d before immunofluorescent quantification of K14/K19 expression.

Cell segmentation with Matlab:

This function imports a directory of pictures, segments cells and cells incorporating EdU from each picture.

Each cell from the cell mode script should be run one after each other.

Initializing cell:

```
input_directory = uigetdir('C:\','Select INPUT directory');
if (input_directory == 0)
error('This directory does not exist');
end
output_directory = input_directory;

%Create excel file names
res_ratio = strcat(output_directory,'/ratio.xls');
res_intensity = strcat(output_directory,'/intensity.xls');
size = 1;
size2 = 1;
count1 =1;
count2 =1;
n1 =1;
n2 =1;
EdU_cKit = zeros(3,2);
EdU_unso = zeros(3,2);
files = dir(input_directory);
```

Cell number 1: Segmenting cells from a picture

```
for i = 1:1:length(files)
% Name of the current picture must contain the population name (cKit,
% or unsorted) and the stiffness (L, M, H, VH, or G)
name = char(files(i).name);

% The directory should contain only pictures, if not, you can select for
% tif or lsm files.

%       if length(name) > 3
%           strin = char(name(length(name)-2:length(name)));
%           % Consider tif files only
%           if strcmp(strin, 'lsm') || strcmp(strin, 'LSM')

disp(strcat('Processing tif stack -',files(i).name,':', num2str(i),'/',...
num2str(length(files))));
```

The coor function finds the population (cKit or unsorted) and the condition (L, M, H, VH, G)

```
[position1,position2] = coor(name);
currentFile = strcat(input_directory, '/', files(i).name);

% Open the current picture
test = imread(currentFile);
% Attribute each channel to a single picture
I_blue = test(:,:,1);
Ired = test(:,:,2);
Igreen = test(:,:,3);
```

```
I_cy = test(:,:,4);

MyRGB = cat(3,Ired,Igreen, I_blue);
MyGray = rgb2gray(MyRGB);
MyEdU = cat(3,Ired,Igreen, I_cy);
I = MyGray;
```

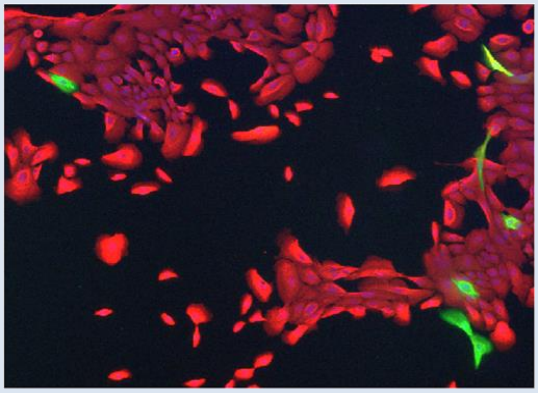

Original picture showing the first three channels (RGB)

The next step is applying a threshold to the picture

```
bw = im2bw(I, 0.08); %This value is flexible

%figure, imshow(bw);
% Fill holes
bw2 = imfill(bw,'holes');
% Remove the objects under 40 pixels
bw4 = bwareaopen(bw2, 40);
```

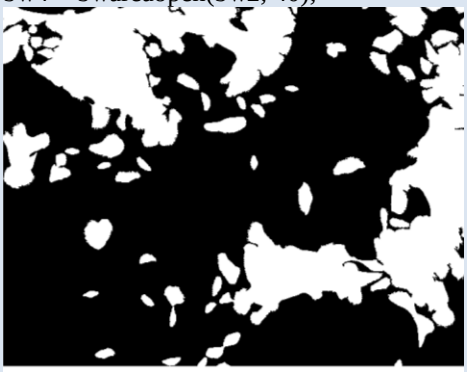

Original picture converted to binary image using a threshold

Getting the perimeter of each object

```
bw4_perim = bwperim(bw4);
```

Finding the nucleus

```
mask_em = imextendedmax(I_blue, 20); %This value is flexible
mask_em = imfill(mask_em, 'holes');
% mask_em = bwareaopen(mask_em, 5);
```

Supplemental information

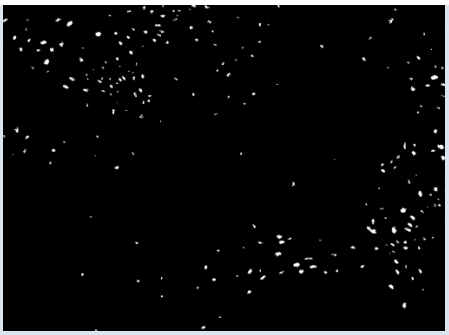

Mask containing the cell nucleus

```
%overlay3 = imoverlay(MyRGB, bw4_perim | mask_em, [.3 1 .3]);
%figure, imshow(overlay3);
```

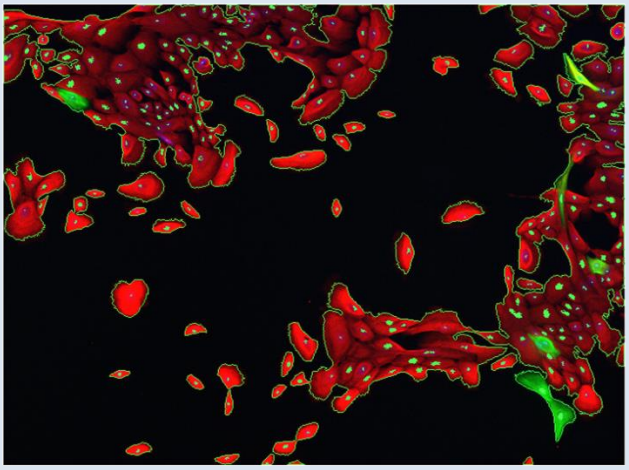

Overlay of the original picture with the perimeter and the marked nucleus

```
% Compute the complement of the picture
I_eq_c = imcomplement(I);
```

Setting regions containing nucleus and background to a minimum

```
I_mod = imimposemin(I_eq_c, ~bw4 | mask_em);
```

Applying the watershed function

```
L = watershed(I_mod);
clear I_mod;
figure, imshow(label2rgb(L))
figure, imshow(MyRGB);
```

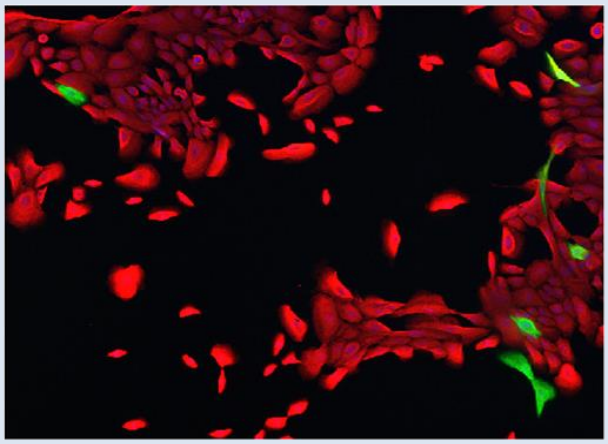

Original picture

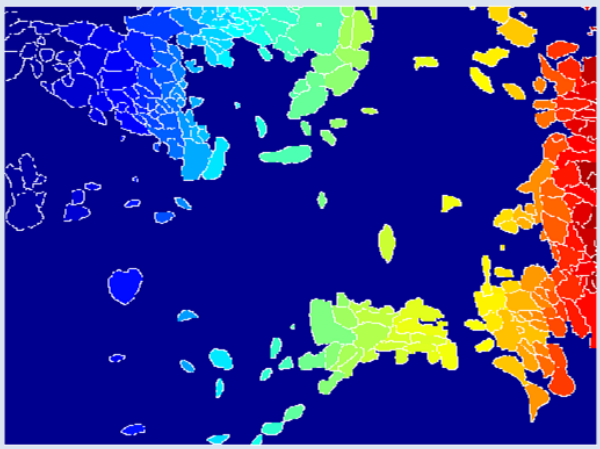

Segmented picture

```
stats = regionprops(L, 'Area', 'Perimeter');
```

```
%Green
stats_green = regionprops(L, Igreen, 'MeanIntensity', 'Area', 'Centroid');
%Red
stats_red = regionprops(L, Ired, 'MeanIntensity', 'Centroid');
%clear L_red;
```

Cell number 2: Segmenting cells incorporating EdU

```
%EdU
bw = im2bw(I_cy, 0.2);
bw2 = imfill(bw,'holes');
bw3 = bwareaopen(bw2, 30);
figure, subplot(2,1,1), imshow(bw3) , subplot(2,1,2), imshow(I_cy);
```

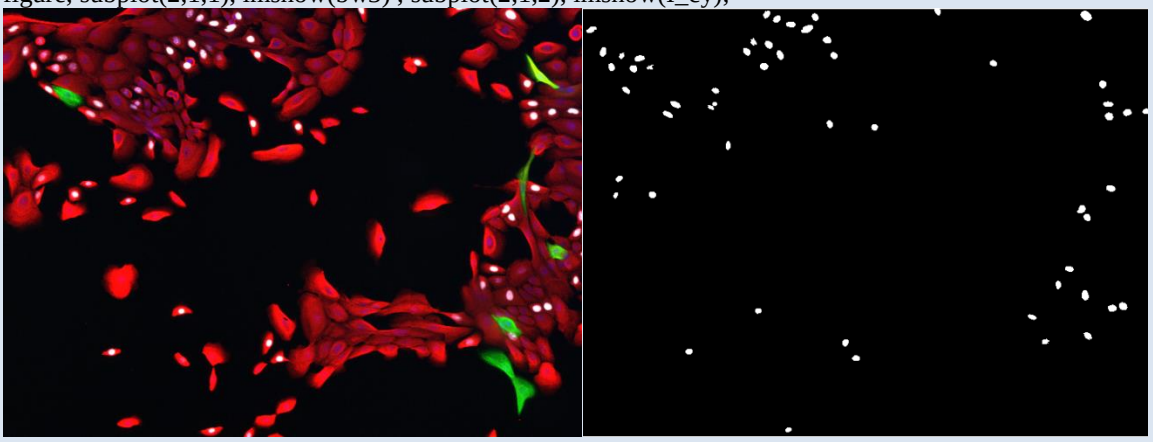

Original picture with nucleus incorporating EdU

Segmented nucleus incorporating EdU

Cell number 3: Computing the number of cells incorporating EdU:

Labeling each object from the segmentation with mean intensitity, area and centroid properties

```
stats_cy5 = regionprops(bw3, I_cy, 'Area','MeanIntensity', 'Centroid');
stats_red2 = regionprops(bw3, Ired, 'MeanIntensity', 'Centroid');
stats_green2 = regionprops(bw3, Igreen, 'MeanIntensity', 'Centroid');

% The EdU function segments cells incorporating EdU and store the red/green
% intensity ratios in a variable.
if position1==1
[EdU_cKit, n2] = EdU(EdU_cKit, n2,position2, stats_red2, stats_green2, stats_cy5);
end

if position1==2
[EdU_unso, n3] = EdU(EdU_unso, n3,position2, stats_red2, stats_green2, stats_cy5);
end
```

Cell number 4: Computing the results

```
m=1;
for k=1:length(stats_green)
% Apply a threshold against the background or unstained cells
if (stats_green(k).Area < 1000) && (stats_red(k).MeanIntensity > 40 ...
|| stats_green(k).MeanIntensity > 40)
if log2(stats_red(k).MeanIntensity / stats_green(k).MeanIntensity ) ~= -Inf ...
```

```
&& log2(stats_red(k).MeanIntensity / stats_green(k).MeanIntensity ) ~= Inf
```

Computing the ratio of each cell and store the intensities

```
ratio(m)=log2(stats_red(k).MeanIntensity / stats_green(k).MeanIntensity );
intensity(m,1) = stats_red(k).MeanIntensity;
intensity(m,2) = stats_green(k).MeanIntensity;

if position1==2 %cKit
histo_cKit(count2,1) = ratio(m);
histo_cKit(count2,2) = position2;
red_cKit(count2,1) = stats_red(k).MeanIntensity;
red_cKit(count2,2) = position2;
green_cKit(count2,1) = stats_green(k).MeanIntensity;
green_cKit(count2,2) = position2;
count1 = count1 +1;
end

if position1==2 %unsorted cells
histo_unso(count3,1) = ratio(m);
histo_unso(count3,2) = position2;
red_unso(count3,1) = stats_red(k).MeanIntensity;
red_unso(count3,2) = position2;
green_unso(count3,1) = stats_green(k).MeanIntensity;
green_unso(count3,2) = position2;
count2 = count2 +1;
end
m=m+1;
end
end
end
```

Writing in different excel files

```
new_size =m;
if exist('ratio')
xlswrite(res_ratio,(Xia, Sakban et al.),'Sheet1', strcat('A',num2str(size)));
xlswrite(res_intensity,{name},'Sheet1', strcat('A',num2str(size2)));
xlswrite(res_intensity,{'Red Intensity'},'Sheet1', strcat('A',num2str(size2+1)));
xlswrite(res_intensity,{'Green Intensity'},'Sheet1', strcat('B',num2str(size2+1)));

xlswrite(res_ratio, ratio','Sheet1', strcat('A',num2str(size+1)));
xlswrite(res_intensity,intensity(:,1),'Sheet1', strcat('A',num2str(size2+2)));
xlswrite(res_intensity,intensity(:,2),'Sheet1', strcat('B',num2str(size2+2)));
xlswrite(res_ratio, position2,'Sheet1', strcat('B',num2str(size+1),':','B',num2str(size+new_size-1)));
size= size + new_size;
size2= size2 + new_size+1;
end
clear ratio;
clear intensity;
%            end
%        end
end
```

Adapted from Steve Eddins, http://blogs.mathworks.com/steve/2006/06/02/cell-segmentation/

Cell feature detection with Matlab:

This function imports a directory of pictures and computes the homogeneity of each picture.

Initializing cell:

```
input_directory = uigetdir('C:\','Select INPUT directory');
if (input_directory == 0)
error('This directory does not exist');
end
output_directory = input_directory;

%Create excel file names
res_ratio = strcat(output_directory,'/ratio.xls');
files = dir(input_directory);
size = 1;
size2=1;
```

Cell number 1: Computing image heterogeneity

```
for i = 3:1:length(files)
% Name of the current picture must contain the population name (cKit,
% or unsorted) and the stiffness (L, M, H, VH, or G)
name = char(files(i).name);
Nmean=[];
% The directory should contain only pictures, if not, you can select for
% tif or lsm files.

%       if length(name) > 3
%           strin = char(name(length(name)-2:length(name)));
%           % Consider tif files only
%           if strcmp(strin, 'lsm') || strcmp(strin, 'LSM')

disp(strcat('Processing image -',files(i).name,':', num2str(i),'/',...
num2str(length(files))));
```

The coor_cyto function finds the population (cKit or unsorted)

```
position = coor_cyto(name);
currentFile = strcat(input_directory, '/', files(i).name);

% Open the current picture
test = imread(currentFile);

% Attribute each channel to a single picture
%blue: Hoechst, red: pFAK, green: phalloidin, mag: vinculin
I_blue = test(:,:,1);
Ired = test(:,:,2);
Igreen = test(:,:,3);
I_mag = test(:,:,4);
I_black = zeros(length(I_blue),length(I_blue));
%In this example, we analyze F-actin homogeneity
MyRGB = cat(3,I_black,Igreen, I_blue);
MyGray = rgb2gray(MyRGB);
```

```
I = MyGray;
```

Filtering the picture

```
H = fspecial('unsharp');
Ish = imfilter(Igreen,H,'replicate');
K = rangefilt(Igreen);
% figure, imshow(K)
% figure, imshow(Igreen)
% figure, imshow(Ish)
```

Applying the graycomatrix function

```
offsets = [ 0 1; 0 2; 0 3; 0 4;...
-1 1; -2 2; -3 3; -4 4;...
-1 0; -2 0; -3 0; -4 0;...
-1 -1; -2 -2; -3 -3; -4 -4];
glcms = graycomatrix(Ish,'Offset',offsets);
stats = graycoprops(glcms,'Contrast Correlation Homogeneity Energy');

Nmean=mean(stats.Homogeneity);
```

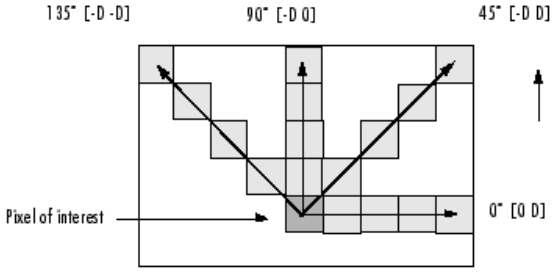

The figure illustrates the spatial relationships of pixels that are defined by this array of offsets, where `D` represents the distance from the pixel of interest.

MathWorks

Adapted from MathWorks: http://www.mathworks.com/help/images/analyzing-the-texture-of-an-image.html

Supplemental References

Ananthanarayanan, B., Y. Kim, et al. (2011). "Elucidating the mechanobiology of malignant brain tumors using a brain matrix-mimetic hyaluronic acid hydrogel platform." Biomaterials **32**(31): 7913-7923.

Ning, X., J. Guo, et al. (2008). "Visualizing metabolically labeled glycoconjugates of living cells by copper-free and fast huisgen cycloadditions." Angew Chem Int Ed Engl **47**(12): 2253-2255.

Xia, L., R. B. Sakban, et al. (2012). "Tethered spheroids as an in vitro hepatocyte model for drug safety screening." Biomaterials **33**(7): 2165-2176.